Friedrich Schiller University

DISSERTATION

Non-Canonical Neuron-Specific Interferon-gamma Pathway in the hSOD1G93A Mouse Model of Amyotrophic Lateral Sclerosis

in partial fulfillment of the requirements for the degree of doctor rerum naturalium (Dr. rer. nat.)

submitted to the Faculty Council of the School of Medicine

by

Saikata Sengupta (M.Sc)

born on 13.12.1988 in Kolkata, India

August 2018

Reviewers:

1. …….
2. …….
3. …….

Date of public disputation:

Table of Contents

LIST OF ABBREVIATIONS

ALS	Amyotrophic lateral sclerosis
AMPA	α-Amino-3-hydroxy-5-methyl-4-isoxazolepropionic acid
ANOVA	Analysis of variance
ATP	Adenosine triphosphate
BDNF	Brain-derived neurotrophic factor
BSA	Bovine serum albumin
Ca^{2+}	Calcium ion
CICR	Calcium-induced calcium release
CNS	Central nervous system
CO_2	Carbon dioxide
CTCF	Corrected total cell fluorescence
C9orf72	Chromosome 9 open reading frame 72
DAPI	4',6-diamidino-2-phenylindole
DMEM/F12	Dulbecco's modified eagle medium: nutrient mixture F-12
DMSO	Dimethyl sulfoxide
ERMCC	Endoplasmic reticulum mitochondria Ca^{2+} cycle
FCS	Fetal calf serum
Fwd	Forward
GAPDH	Glyceraldehyde-3-phosphate dehydrogenase
GAS	Gamma activated site
GluR1	Glutamate receptor 1 subunit
GluR2	Glutamate receptor 2 subunit
HBSS	Hank's balanced salt solution
HEPES	4-(2-Hydroxyethyl)-1-piperazineethanesulfonic acid
hmbs	hydroxymethylbilane synthase
IFN-	Interferon gamma
© IFN-	Interferon gamma receptor 1 subunit
©R1	Interferon gamma receptor 2 subunit
IFN-©R2	Interferon gamma receptor complex
IFN-©R	Interleukin
IL	1,4,5-triphosphate receptors
IP_3R	Janus kinase 1
JAK1	Kainate
KA	Laser scanning microscopy
LSM	Mitochondrial Uniporter
MCU	Major histocompatibility complex
MHC	Mitochondrial sodium/calcium exchanger
mNCE	Mitochondrial permeability transition pore
mPTP	Messenger ribonucleic acid
mRNA	Phosphorylated neurofilament heavy chain
pNfH	Neurofilament light chain
NfL	Non-transgenic
Nontg	Phosphate buffered saline
PBS	Polymerase chain reaction
PCR	Paraformaldehyde
PFA	Protein Kinase A
PKA	

I

qPCR	Quantitative polymerase chain reaction
Rev	Reverse
ROS	Reactive oxygen species
RT	Room temperature
RyR	Ryanodine receptors
SDS	Sodiumdodecyl sulfate
SERCA	Sarco/endoplasmic reticulum calcium-ATPase
SOD1	Superoxide dismutase 1
STAT1	Signal transducer and activator of transcription 1
UK	United Kingdom
USA	United States of America
VDAC	Voltage dependent anion channel

Units

hr	hour
L	litre
µL	microlitre
mL	millilitre
M	molar (moles/litre)
nM	nanomolar (nanomoles/liter)
µM	micromolar (micromoles/liter)
mM	millimolar (millimoles/liter)
µm	micrometer
U	Units
s	seconds
%	percent
°C	degree Celsius

SUMMARY

Amyotrophic Lateral Sclerosis (ALS) is the most commonly occurring motor neuron disease that is fatal and incurable. Motor neurons are markedly vulnerable to excitotoxicity mostly from over-stimulation of alpha-amino-3-hydroxy-5-methyl-4-isoxazolepropionic (AMPA) receptors and are principal targets in ALS. Interferon-gamma (IFN-γ), a pro-inflammatory cytokine, can independently cause neuronal dysfunction by triggering calcium influx through a calcium-permeable complex of IFN-γ receptor 1 (IFN-γR1) subunit and AMPAR subunit Glutamate Receptor 1 (GluR1). This receptor complex is formed via a non-canonical neuron-specific IFN-γ pathway.

In this study, we explore the expression of the non-canonical IFN-γ pathway's key participants – the upstream targets: IFN-γR1 and GluR1, and the downstream players: Janus Kinase 1(JAK1), Signal Transducer and Activator of Transcription (STAT1), and Protein Kinase A (PKA) – for the first time in the hSOD1G93A ALS mouse model. Elevated IFN-γR1 protein expression was observed in motor neurons of both presymptomatic and symptomatic hSOD1G93A, while GluR1 protein levels were higher only in the symptomatic ALS mice *ex vivo*. The expression of the downstream participants, namely JAK1 and STAT1, were unchanged irrespective of age group and genotype, while one of PKA's catalytic subunits was downregulated at transcript level in hSOD1G93A mice. In *in vitro* system involving primary motor neuron-enriched co-cultures representing the embryonic stage, IFN-γR1 and GluR1 were similarly expressed in both hSOD1G93A mice and non-transgenic control mice.

We, also, determined the direct effects of IFN-γ alone or in the presence of an excitotoxic agent, kainate, on motor neuron survival *in vitro*. IFN-γ was weakly neurotoxic on the embryonic motor neurons and did not influence kainate-mediated excitotoxicity.

In conclusion, increased IFN-γR1 in motor neurons of adult hSOD1G93A mice can most likely sensitize the neurons to excitotoxic insults involving GluR1 and/or pathways mediated by IFN-γ, thus, serving as a potential direct link between neurodegeneration and inflammation in ALS.

ZUSAMMENFASSUNG

Amyotrophe Lateralsklerose (ALS) ist die am häufigsten auftretende Motoneuronerkrankung, die sowohl tödlich als auch unheilbar ist. Motoneurone, die Hauptziele in ALS, sind besonders anfällig für Exzitotoxizität, welche vor allem aus Überstimulation von alpha-amino-3-hydroxy-5-methyl-4-isoxazolepropionic (AMPA) Rezeptoren hervorgeht. Interferon-gamma (IFN-γ), ein proinflammatorisches Zytokin, kann unabhängig neuronale Dysfunktion verursachen, in dem es Calciumeinstrom durch einen Calcium-permeablen Komplex der IFN-γ Rezeptor 1 (IFN-γR1) Untereinheit und der AMPAR Untereinheit Glutamat Rezeptor 1 (GluR1) auslöst. Dieser Rezeptorkomplex wird durch einen unkonventionellen, neuronspezifischen Signalweg geformt.

In dieser Studie untersuchen wir die Expression der Schlüsselfaktoren des unkonventionellen IFN-y Signalweges: die vorgeschalteten Ziele IFN-γ und GluR1 sowie die nachgeschalteten Faktoren Janus Kinase 1(JAK1), Signal Transducer and Activator of Transcription (STAT1) und Protein Kinase A (PKA) - zum ersten Mal im hSOD1G93A ALS Mausmodell. Erhöhte IFN-γR1 Proteinexpression wurde sowohl bei präsymptomatischen als auch symptomatischen Motoneuronen der hSOD1G93A Mäuse beobachtet, während GluR1 Proteinlevel nur in den symptomatischen ALS Mäusen ex vivo erhöht waren. Die Expression der nachgeschalteten Beteiligten JAK1 und STAT1 war unabhängig von Alter und Genotyp unverändert, während eine katalytische Untereinheit der PKA in hSOD1G93A Mäusen herunter reguliert war. Im in vitro System, das primäre Motoneuron-angereicherte Kokulturen enthält, die die embryonale Phase repräsentieren, waren IFN-γR1 und GluR1 sowohl in hSOD1G93A Mäusen als auch nicht-transgenen Kontrollmäusen gleich exprimiert. Weiterhin ermittelten wir den direkten Einfluss von IFN-γ allein und in Kombination mit der exzitotoxischen Substanz Kainat auf Motoneuronüberleben in vitro. IFN-γ wirkte schwach neurotoxisch auf die embryonalen Motoneurone und übte keinen Einfluss auf die Kainat-vermittelte Exzitotoxizität aus.

Zusammenfassend ist die erhöhte Expression von IFN-γR1 in Motoneuronen erwachsener hSOD1G93A Mäuse höchstwahrscheinlich in der Lage, Neurone für GluR1 und/oder IFN-γ vermittelte Signalwege bedingte Exzitotoxizität zu sensibilisieren. Dies lässt auf eine potentielle direkte Verbindung zwischen Neurodegeneration und Entzündung in ALS schließen.

1. INTRODUCTION

Neurodegenerative diseases collectively refer to a diverse group of disorders that are defined by chronic progressive loss of neurons in specific regions of the human central nervous system, resulting in functional impairments. They are debilitating, incurable, widely prevalent, and include conditions like Alzheimer's disease, Parkinson's disease, and Amyotrophic Lateral Sclerosis. Most of these diseases are late-onset and affect the elderly.

The central nervous system (CNS), originally considered to be immune-privileged, is now recognized to have a unique actively monitoring immune system. In neurodegenerative conditions, immune activation involves the resident immune cells of the CNS, namely, astrocytes and microglia. Initially, the immune responses are acute and typically neuroprotective, which later progress to chronic, deleterious kind. These responses trigger neuroinflammation that in turn drives neurodegeneration, thus, resulting in a vicious degeneration-inflammation cycle.

In this thesis, the general objective was to examine a molecular pathway that could be a direct link between neurodegeneration and neuroinflammation in the neurodegenerative disease Amyotrophic Lateral Sclerosis (ALS).

1.1 General Introduction to ALS

Amyotrophic Lateral Sclerosis or Lou Gehrig's disease, the most frequent motor neuron disease in the world, is a rapidly progressive lethal neurodegenerative disorder destroying both the upper and lower motor neurons of the CNS. ALS has an annual incidence of 1-2.6 cases per 100,000 individuals and an average onset age of 58-60 years (Talbott *et al.*, 2016). Patients typically survive 3-4 years post onset and death is mostly due to loss of voluntary muscle function, leading to paralysis and respiratory failure. Despite several years of research, the disease is yet to find a cure, mostly because of its complex etiology. Thus, studies for better understanding of the pathomechanism of this disease are deemed important to identify potential therapeutic targets.

1.1.1 Diagnosis and treatment of ALS

Clinically, amyotrophic lateral sclerosis patients mostly present with asymmetric limb weakness in the 5th or 6th decade of their lives that progress to symmetric peripheral muscle paralysis. The limb weakness is observed as deficits in fine motor skills, which is typically initially noted in the fingers. This kind of ALS is referred to as limb or spinal-onset ALS (Swinnen & Robberecht, 2014) and is, also, the classical form in which the upper extremities of the patients are first affected followed by gradual contralateral spread. Signs of motor neuron damage in spinal ALS continue to unfold in the contralateral and ipsilateral lower extremities as the disease progresses. Head-neck or bulbar-onset ALS, which is characterized by symptoms like dysphagia and dysarthria, has fewer cases (20-25%) and are more severe with mortality in about 2 years (Figure 1). Irrespective of the onset-type, the clinical features typically include muscle atrophy, weakness, spasticity, fasciculations, and hyperreflexia. The manifestations are a result of damage to both upper motor neurons (UMNs) present in the corticospinal tract and lower motor neurons (LMNs) that innervate the muscles. The disease course ultimately culminates with paralysis and death from respiratory failure.

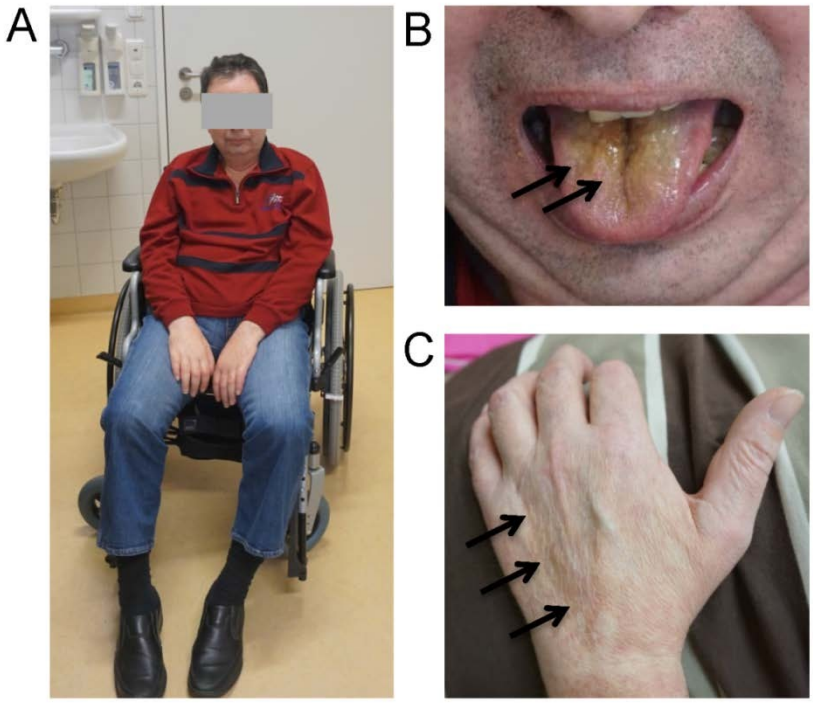

Figure 1. Typical symptoms of a patient with ALS. (A) A 64 year old man suffering from ALS with progressive muscle weakness. (B) Bulbar tongue twitching. (C) Hand muscle atrophy of 60 year old man with ALS. With permission. Hans Berger Department of Neurology, University Hospital, Jena.

Two other rare forms of the disease are peroneal ALS that has a spreading pattern of lower-upper extremity and respiratory musculature onset ALS causing very early death (Daroff *et al.*, 2012). Interestingly, the motor neurons that control ocular movement and urethral or external anal sphincters remain unaffected throughout the entire disease course (Eisen &

Weber, 2001). Moreover, ALS has been recently confirmed to be associated with Frontotemporal Dementia (FTD), with a frequency of 5%-40% (Ferrari *et al.*, 2011). Frontotemporal Dementia refers to a group of disorders defined by degeneration of basal ganglia and cerebral cortex neurons, thus, leading to cognitive, language, and behavioural deficits (Burrell *et al.*, 2016). An ALS/FTD association implies overlapping molecular pathways critically involved in disease pathogenesis (Weishaupt *et al.*, 2016). These revelations strongly present the complexity of ALS diagnosis.

As per the revised El Escorial Criteria for ALS, the disease diagnosis requires the following: clinical assessment and presence of both lower and upper motor neuron damage, an evident advancement in symptoms, and the omission of disease mimics and other causes based on relevant pathological, neuroimaging, and electrophysiological evidence. Electromyography, the only method that can diagnose ALS in its early stages, can reveal active and chronic muscle denervation. Currently, there are no blood tests or definitive group of ALS biomarkers that could aid diagnosis. The only ALS biomarkers known till date are the phosphorylated neurofilament heavy chain (pNfH) and neurofilament light chain (NfL) proteins whose levels vary in cerebrospinal fluid and blood serum of ALS patients (Poesen *et al.*, 2017)

In terms of disease progression, it is critical to note that the advancement is both curvilinear and highly variable from patient to patient (Gordon *et al.*, 2010). Existing ALS therapy comprises of various components: drug treatments, physical therapy, and symptomatic therapy. Presently, there are no commercially available drugs available to cure ALS. The only medications available work mostly in slowing the disease progression when administered in the early stages. Riluzole has been the drug longest in use for ALS until the recent US FDA approval of another drug, Edaravone. While the former is known to control excitotoxic death, the latter drug most likely works via its antioxidant properties.

1.1.2 ALS pathogenesis

Given the complexity and heterogeneity of ALS, we currently have no unifying explanation for its pathogenesis. As previously stated, motor neurons are the primary targets with collateral damage to the glial population to an extent wherein the latter gets involved in exacerbating the disease condition.

Motor neuron degeneration in ALS has been attributed to multiple factors that occur in cohesion or succession: calcium dysregulation, excitotoxicity from excessive glutamatergic receptor stimulation, neuroinflammation, endoplasmic reticulum stress, mitochondrial dysfunction, aberrant RNA processing, defective axonal trafficking, excessive protein aggregation and reactive oxygen species (ROS) generation amongst others (Cozzolino *et al.*, 2012; Tadic *et al.*, 2014; Taylor *et al.*, 2016).

Based on genetics, ALS can be sporadic or familial depending on the presence of identified inheritable ALS mutated genes. The disease is mostly sporadic and comprises approximately 90% of the cases. Familial ALS occurrence is due to inheritance of mutations in a mostly autosomal-dominant manner. Since the identification of first ALS mutation in SOD1 gene for familial ALS, more than 20 ALS linked genetic loci have been identified. The most frequently reported ALS inherited mutations are those in C9orf72 (~35% cases), a hexanucleotide repeat expansion, and SOD1 (~20% cases) (Kirby *et al.*, 2016; Taylor *et al.*, 2016).Interestingly, several genetic mutations in familial ALS have also been identified in sporadic cases, especially those in C9orf72 (Kirby *et al.*, 2016)

Of the various pathogenic factors contributing to ALS, excitotoxicity and neuroinflammation have long been implicated in disease progression. A pathological process in which neurons are damaged or killed from excessive stimulation of their receptors for excitatory glutamate, excitotoxicity is a kind of neurotoxicity implicated in several neurodegenerative conditions (Dong *et al.*, 2009). Glutamate, the chief excitatory brain neurotransmitter, takes part in this kind of neuronal death. Apart from impaired glutamate receptor or relevant ion channel functioning, this kind of excitotoxicity can be due to excessive glutamate release and poor astrocytic glutamate uptake (Grosskreutz *et al.*, 2010; King *et al.*, 2016). One of the principal receptors for glutamate is AMPARs (α-amino-3-hydroxy-5-methyl-4-isoxazolepropionic acid receptors) that are composed of four subunits: GluR1, GluR2, GluR3, and GluR4. They are

typically heterotetrameric wherein two of the four subunits are present as pairs (dimer of dimers) (Mayer, 2005; Greger *et al.*, 2007). Under physiological conditions, the calcium-permeable AMPAR stimulation causes calcium influx that activates different signaling pathways for neuronal functioning. In pathological cases, over-activation of these receptors causes enormous calcium influx that disturbs intracellular homeostasis and drives the cells towards apoptosis.

This type of neuronal death from excessive calcium influx is due to disruption of the Endoplasmic Reticulum Mitochondria Calcium Cycle (ERMCC) that is involved in regular calcium buffering dynamics in motor neurons (Grosskreutz *et al.*, 2010; Cozzolino *et al.*, 2012; Tadic *et al.*, 2014).

The shuttling of calcium between the ER and mitochondria appears to occur in a cyclic manner (Grosskreutz *et al.*, 2010; Cozzolino *et al.*, 2012; Tadic *et al.*, 2014), which is referred to as the ERMCC (Figure 2). Under physiological conditions, AMPAR stimulation triggers an increase in cytosolic calcium, which in turn is pumped into the ER through the sarco/endoplasmic reticulum Calcium-ATPase (SERCA). The motor-neuronal ER stores around 5 times higher magnitude calcium as compared to that present in the cytoplasm (Stutzmann & Mattson, 2011). This stored calcium could be used to modulate the excitability, signal amplification, and neurotransmitter release from the neuron, apart from synchronization of post-translational protein editing with the energy supplied by the ERMCC (Verkhratsky, 2005; Gunter & Sheu, 2009; Grosskreutz *et al.*, 2010). The pumping in of calcium induces calcium release from the ER stores through the ryanodine receptors (RyR) and 1,4,5-triphosphate receptors (IP_3Rs) and the process is called Calcium-Induced Calcium Release (CICR). This is followed by uptake of calcium by the mitochondria chiefly via the Mitochondrial Uniporter (MCU) complex, which is facilitated by the large negative membrane potential of the mitochondria. This organelle is known to buffer the lion's share of intracellular calcium in motor neurons. The fact that the blocking of mitochondrial calcium buffering quickly depresses neurotransmitter release emphasizes the importance of mitochondria in motor-neuronal calcium buffering (Grosskreutz *et al.*, 2010). The accumulated calcium is then slowly released back into the cytosol via the mitochondrial sodium/calcium exchanger (mNCE) or the transient opening of the mitochondrial permeability transition pore (mPTP), only to be later taken up by the ER via the SERCA (Tadic *et al.*, 2014).

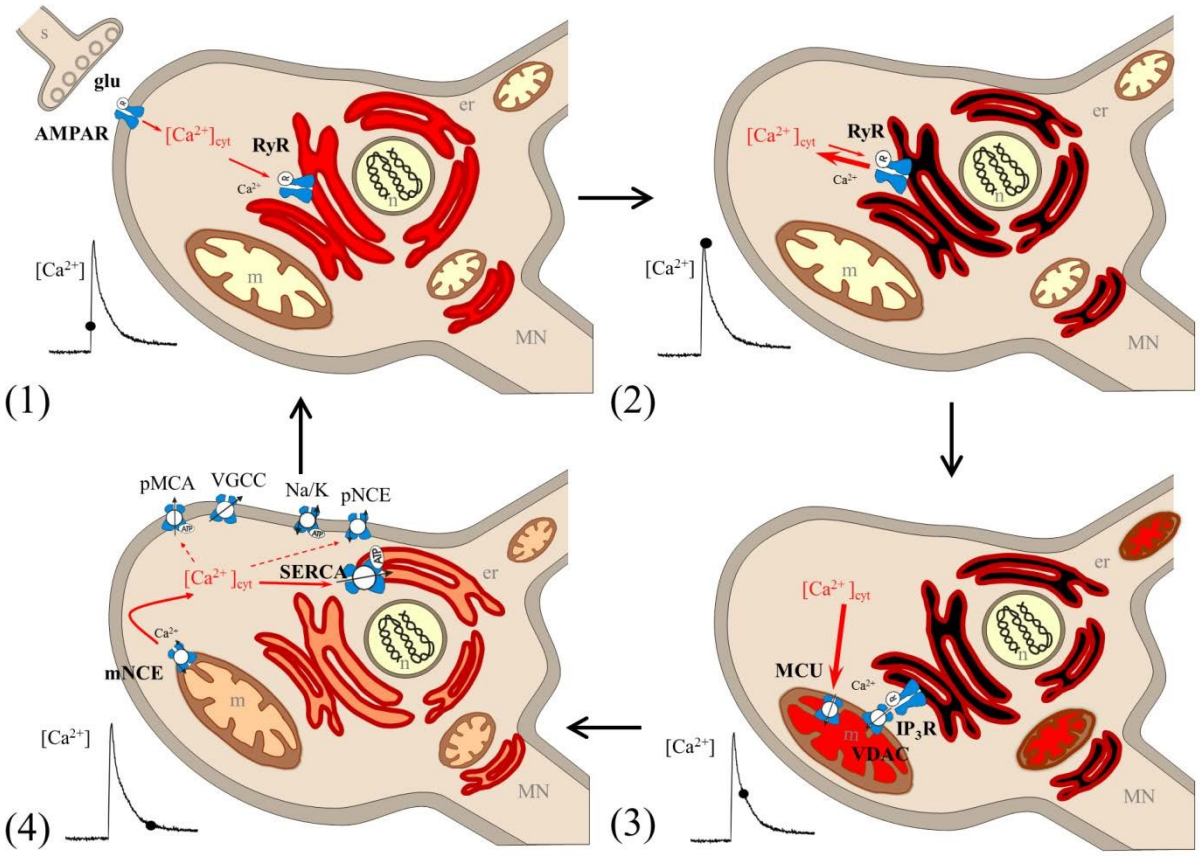

Figure 2. Simplified representation of the ERMCC under physiological conditions (1) Following α-Amino-3-Hydroxy-5-Methyl-4-Isoxazolepropionic Acid receptor (AMPAR) stimulation, calcium (Ca^{2+}) enters the cytosol. (2) Ryanodine receptor (RyR) on the ER membrane senses the increase in cytosolic Ca^{2+} and releases more Ca^{2+} from the ER (through a process called Ca^{2+}-induced Ca^{2+} release). (3) ER Ca^{2+} is released through 1,4,5 trisphosphate receptor (IP_3R), too. Voltage dependent anion channel (VDAC), present in the outer mitochondrial membrane, uptakes cytosolic Ca^{2+} and can directly take up portion of the released Ca^{2+} from the ER as well. Most of the cytosolic Ca^{2+} uptake by the mitochondria takes place through the mitochondrial Ca^{2+} uniporter (MCU) complex, which is present in the inner mitochondrial membrane. (4) Ca^{2+} is released from the mitochondria via the mitochondrial sodium Na^+/Ca^{2+} exchanger (mNCE). Refilling of the ER Ca^{2+} stores occurs through the sarco/endoplasmic reticulum Ca^{2+}-ATPase (SERCA). Additionally, cytosolic Ca^{2+} is cleared by the plasma membrane Ca^{2+}-ATPase (PMCA) and the plasma membrane Na^+/Ca^{2+}exchanger (pNCE).

In the case of ALS, excessive stimulation of AMPARs results in high levels of cytosolic calcium that leads to a chronic shift of calcium from ER stores to the mitochondria. While

abnormally low levels of ER calcium lead to misfolding of proteins, mitochondrial calcium overload generates ROS and releases mitochondrial contents like stored ions into the cytosol via the mPTP and mNCE (Crompton, 1999; Gunter & Sheu, 2009; Grosskreutz *et al.*, 2010; Barrett *et al.*, 2014; Brini *et al.*, 2014; Tadic *et al.*, 2014). This activates Bcl-2 dependent apoptotic mechanisms that lead to neuronal death. The glutamate released from damaged neurons or synaptic clefts extends further damage by acting on surrounding neurons (Choi, 1988). Motor neurons are particularly vulnerable to excitotoxic death owing to high number of calcium-permeable AMPARs as against low number of intracellular calcium buffering proteins like parvalbumin and calbindin d-28k and low mitochondrial density per cell volume (Grosskreutz *et al.*, 2007; Tadic *et al.*, 2014). These attributes of motor neurons are particularly pronounced in ALS, thus, defining AMPAR excitotoxicity mediated by the ERMCC as a key pathogenic mechanism in the disease that drives neurodegeneration (Van Den Bosch *et al.*, 2006).

Concomitant with neurodegeneration is neuroinflammation, a chronic over-activation of the CNS immune system, which exacerbates the damage in ALS. Initially neuroprotective in nature, the immune responses soon become toxic, thus, serving as catalysts to the disease progression. While there is a distinct activation or expansion of glial cells both *in vitro* and *in vivo*, T-lymphocytes have, also, been seen to infiltrate the brains and spinal cords of ALS cases at different stages of the disease (Philips *et al.*, 2011). Intercellular communication between the neurons, glia, and lymphocytes is critical in understanding the complexity of the disease pathogenesis.

1.1.3 ALS mouse model with SOD1 mutation: hSOD1G93A

The best and most widely used mouse model for the study of motor neuron death in ALS is the one that mimics the onset, progression, and severity of the human disease by gross overexpression (15-20 copies) of human SOD1 transgene having a missense mutation of guanine to alanine substitution at position 93, namely the hSOD1G93A gene (Gurney *et al.*, 1994). These mice demonstrate 40-50% motor neuron loss in the lumbar spinal cord by disease end stage prior to considerable retraction of nerve terminals from the neuromuscular junction.

The SOD1 gene encodes superoxide dismutase-1, a ubiquitously expressed cytosolic enzyme that scavenges harmful superoxide radicals. Over 150 mutations in the SOD1 have been associated with ALS that fascinatingly occur throughout the length of the protein rather than being confined to a specific functional domain (Kirby *et al.*, 2016). Considering that mice lacking SOD1 do not exhibit motor neuron disease (Reaume *et al.*, 1996), this hSOD1G93A mouse model suggests that the role of SOD1 gene in ALS is less likely to be a loss of regular enzymatic function, but rather a gain of toxic function of the protein.

The hSOD1G93A mouse has been a subject of criticism in ALS research, principally because of the profound transgene overexpression (15-20 copies) required to recapitulate the disease and the shortage of experimental findings from the model that have translated therapeutically to the human condition (Zwiegers & Shaw, 2015). Nevertheless, the hSOD1G93A mouse remains one of the most well-characterized and widely-used mouse models for both neurodegeneration and inflammation studies in ALS. Moreover, considering that the study focuses on the effect of IFN-γ on motor neurons, it was imperative to employ this mouse model that recapitulates motor neuron death very well and expresses high levels of pro-inflammatory cytokines like IFN-γ.

1.2 General Introduction to IFN-γ signaling

Interferon-gamma (IFN-γ) is one of the key cytokines involved in immune and inflammatory responses. Its precise role in the central nervous system is still unclear and appears to involve a miscellaneous set of responses from different cell types. In the case of neurons, the direct effects of this cytokine are yet to be well delineated (Kulkarni *et al.*, 2016). While some studies demonstrate its pro-survival role in neurons (Barish *et al.*, 1991; Song *et al.*, 2005; O'Donnell *et al.*, 2015), others report detrimental consequences (Kim *et al.*, 2002; Mizuno *et al.*, 2008). In the following sections, the cytokine is discussed along with its canonical and non-canonical pathways relevant to this study.

1.2.1 Interferon gamma (IFN-©)

Interferons (IFNs) were basically described as molecules released by cells to defend viral infection (Farrar & Schreiber, 1993). Based on their cellular source, biological functions, gene structure, and the like, this group of signaling proteins is subdivided into 2 classes: Type I and

Type II. Type I IFNs are typically generated in response to viral infection. This class of IFNs is further divided into two: IFN-α family synthesized largely by leukocytes and IFN-β single protein largely produced by fibroblasts. IFN-© is Type II IFN that is primarily induced by inflammatory and immune stimuli and exclusively produced by T-lymphocytes and natural killer cells (Schoenborn & Wilson, 2007).

IFN-© is a pleiotropic cytokine that promotes both specific and general host defense mechanisms against infections and tumors (Farrar & Schreiber, 1993). As compared to Type I IFNs, IFN-© plays a more exhaustive role in immunomodulation like upregulating Major Histocompatibility Class (MHC)-I, inducing MHC-II expression, regulating mononuclear phagocytes and humoral immune responses, and synthesis of certain proinflammatory or immunomodulatory cytokines (Farrar & Schreiber, 1993). In the lines of inflammation, IFN-© is an effector cytokine that regulates macrophage activation (phagocytic immune cell) via JAK (Janus kinase)/STAT (Signal Transducer and Activator of Transcription) signaling, a pathway that is explained later in this chapter. IFN-© drives the macrophages towards the killer "M1" phenotype that leads these cells to express high levels of pro-inflammatory cytokines such as TNF-α (Tumor Necrosis Factor-〈), IL(Interleukin)-1®, IL-12, and IL-23 and generate excessive reactive nitrogen and oxygen species (Martinez & Gordon, 2014). These events promote strong inflammatory activity. It would be appropriate to note at this point that microglia, one of the key immune cells of CNS and participants in ALS progression, are resident macrophages of the brain and spinal cord and follow the mentioned activation pattern.

In terms of IFN-© expression in the CNS, elevated levels of IFN-© was observed in the cerebrospinal fluid and serum of ALS patients and the values correlated with disease progression (Liu *et al.*, 2015). Similarly, this cytokine was shown to be significantly increased in both the spinal motor neurons and astrocytes of hSOD1G93A mouse at disease onset and symptomatic stage (Michaelson *et al.*, 2017). Thus, these studies strongly suggest the possibility of upregulated IFN-© pathways in the CNS of ALS cases.

1.2.2 IFN-γ receptor complex and canonical IFN-γ signaling

The functional interferon gamma (IFN-©) receptor complex comprises of two glycoprotein chains: ligand-binding subunit and signal transducing component. While the former is often referred to as IFN-©R1, IFN-© receptor α chain, or CDw119, the latter is known as IFN-©R2, IFN-© receptor β chain or accessory factor-1 (AF-1) (Bach *et al.*, 1997).

IFN-©R1 binds to its ligand, IFN-©, with a high affinity (K_a) of 10^9-10^{10} M^{-1} with most of the extracellular domain (6-227 residues) involved in the activity. This induces rapid dimerization of IFN-©R1 subunits resulting in a site that is recognized by the extracellular domain of the IFN-©R2 subunits. The dimerization of IFN-©R1 and IFN-©R2 brings the two receptor-associated JAKs (Janus Kinases) closer to transactivate and phosphorylate the receptor units. This is supported by research that shows the inability of IFN-©R2 to transduce signals in response to IFN-© when its JAK2 association site is deleted. Crystallographic studies show that the functional IFN-©: IFN-©R complex comprises of the IFN-© homodimer bound to two JAK1-associated IFN-©R1 and two JAK2-associated IFN-©R2 chains (Bach *et al.*, 1997; Pestka *et al.*, 1997). Transphosphorylation of receptor subtypes by the JAKs is followed by phosphorylation of Tyr^{440} in IFN-©R1 by either of the kinases. The phosphorylated segments from both the IFN-©R1 chains recruit two molecules of STAT1α, which are then phosphorylated by JAK1 and JAK2. This results in the formation of functional phosphorylated STAT1 (pSTAT1) homodimer that translocates to the nucleus. Subsequently, pSTAT1 binds to DNA sequences called the gamma interferon activated site (GAS) with high affinity to start transcription of interferon stimulated genes (Shuai *et al.*, 1992; Muller *et al.*, 1993; Darnell *et al.*, 1994; DECKER *et al.*, 1997). In parallel, acetylation of pSTAT1 defines the time point for STAT1 inactivation wherein complex formation occurs between acetylated STAT1 and the phosphatase T-cell protein called tyrosine phosphatase (Krämer *et al.*, 2009). Finally, histone deacetylase 3 deacetylates STAT1 protein, thus, releasing it to participate in a new cycle of stimulation and reactivation (Chen *et al.*, 2012).

Both the types of IFN-©R subunits belong to cytokine class II receptor superfamily. In their dimerized state, the IFN-©R1 chains are 27 Å apart and do not interact with each other

(Walter *et al.*, 1995). This explains the inability of the IFN-©R1 dimer to induce signaling

independently despite the presence of both a JAK1 association site and a Stat1〈 recruitment site as the physical distance prevents transphosphorylation of the receptor units.

In terms of expression, studies suggest that the levels of the two IFN-©R subunits varies greatly across cell types. IFN-©R1 seems to be constitutively expressed on the surfaces of nearly all types of cells at moderate levels. In contrast, IFN-©R2 shows extremely low constitutive expression with its gene's transcription under possible tight regulation (Pernis *et al.*, 1995; Bach *et al.*, 1997). IFN-©, also, appears to regulate IFN-©R2 levels in certain cell types (Bach *et al.*, 1997). Surface expression of the fully mature protein differs greatly among tissues and, apparently, there is no direct correlation between extent of IFN-©R1 expression and degree of IFN-© induced response (Farrar & Schreiber, 1993). The IFN-©R1 gene is encoded on chromosome 6q for humans and chromosome 10 for mouse, while the IFN-©R2 is encoded on chromosome 21q for humans and 16 for mouse (Hibino *et al.*, 1991; Cook *et al.*, 1994; Soh *et al.*, 1994). Overall speaking, although IFN-©R complex is ubiquitously present in cells, the role of the receptor is complex and not, yet, very well understood: for example, the reason behind its inability to support all known actions of IFN-© is still under investigation.

1.2.3 Neuron-specific non-canonical IFN-γ pathway regulating calcium

Apart from the classical IFN-γ signaling involving JAK1/STAT1, there are several other non-canonical IFN-γ pathways that may or may not be STAT1 dependent. The functioning of these pathways is cell and context-dependent. Existence of these pathways presents the complexity of IFN-γ signaling and varied roles of the cytokine both in immune and inflammatory responses.

In neurons, IFN-γ is known to induce neurotoxicity through a non-canonical pathway involving IFN-γR1 and GluR1 subunits from IFN-γR and AMPAR respectively that causes increased calcium influx. Several studies report the ability of IFN-γ to directly induce calcium transients possibly via calcium channels or by opening intracellular calcium stores in different cell types (Hansen ' *et al.*, 1994; Kung *et al.*, 1995; Martino *et al.*, 1996; AAS *et al.*, 1998; Franciosi *et al.*, 2002). In neurons, however, the cytokine triggers calcium influx by inducing a calcium-permeable receptor complex formation between IFN-γR1 and GluR1 as was

demonstrated in mouse cortical neurons *in vitro* (Mizuno *et al.*, 2008). The cytokine binds to IFN-γR1, which results in activation of downstream JAK1/STAT1. Activated STAT1 mediates elevation in cAMP levels via adenylyl cyclase activity leading to activation of PKA (Protein Kinase A). Finally, PKA mediates the IFN-γR1:GluR1 complex formation by phosphorylating GluR1 at serine 845 position (Figure 3). Increased calcium influx elevates intracellular nitric oxide levels that damage the mitochondria, thus, resulting in drop in ATP levels and subsequent neuronal damage.

The ability of IFN-γR1 to couple with neuron-specific calcium permeable AMPAR presents a potential neurotoxic mechanism that can play a role in both neurodegenerative and inflammatory diseases. In this study, we examine the pathway in the context of ALS using the mouse model hSOD1G93A.

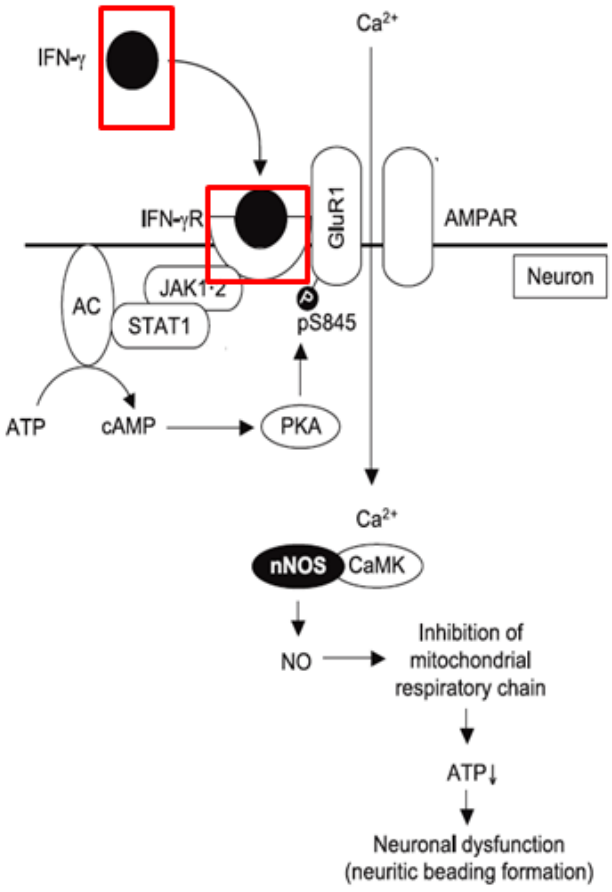

Figure 3. IFN-γR1:GluR1 pathway. Mizuno, T., et al. (2008). "Interferon-gamma directly induces neurotoxicity through a neuron specific, calcium-permeable complex of IFN-gamma receptor and AMPA GluR1 receptor." FASEB J 22(6): 1797-1806. IFN-γ binding to IFN-γR activates Jak1/STAT1 signaling that elevates cAMP levels from increased adenylyl cyclase (AC) activity and activates PKA. Phosphorylation of GluR1 by PKA at serine-845 induces calcium-permeable receptor complex formation with IFN-γR1 and increased calcium influx leads to enhanced nitric oxide production. This results in neuronal dysfunction via inhibition of mitochondrial respiratory chain.

2. AIMS OF STUDY

This study's hypothesis is principally based on two well-established facts: First, motor neurons are particularly susceptible to excitotoxic death owing to high number of AMPARs and low levels of calcium buffering proteins. Second, IFN-γ independently induces calcium influx in neurons by initiating a neuron-specific calcium permeable complex formation involving IFN-γR1 and AMPAR subunit GluR1. Considering that IFN-γ holds the potential to enhance neuronal death in a fashion akin to AMPARs, examining this cytokine and its receptor can serve as a possible direct link between neurodegeneration and neuroinflammation in ALS.

The study examines this calcium-transients inducing non-canonical IFN-γ pathway in motor neurons from both non-transgenic and hSOD1G93A mice. Reckoning the potential of AMPAR and IFN-γR stimulation in triggering neurotoxicity, the hypothesis is that the IFN-γ inducing motor neuron damage would be observed in both mouse systems, with a special element of aggravation in hSOD1G93A mice.

On these lines, the aims of this study include the following:

- examine the expression levels of the primary targets, IFN-γR1 and GluR1, *in vitro*
- demonstrate the effect of IFN-γ on motor neuron survival *in vitro*
- study the cytokine's influence in regulating calcium levels in motor neurons *in vitro*

Apart from examining primary mouse motor neurons *in vitro* that is representative of embryonic stage, this study gathered insights on the pathway's participants in the adult mice, *ex vivo*. For this, the following were examined in the motor neurons of hSOD1G93A mice, both before and after disease onset, alongwith those of age-matched non-transgenic adult mice:

- expression of upstream targets, IFN-γR1 & GluR1
- levels of downstream targets JAK1, STAT1, and Protein Kinase A

For expression studies, both mRNA and protein levels were measured. The functional studies to determine the effects of IFN-γ *in vitro* comprised of cell survival study and single-cell calcium measurements.

3. MATERIALS AND METHODS

3.1 Animals

All animal care, husbandry, and experimentation were performed according to the guidelines set by the Directives of the Protection of Animals Act and agreed upon by the animal welfare authorities of Thuringia, Germany (accreditation number: 02-046/14). Mice were monitored regularly for motor impairment and euthanized upon onset of major paralysis to alleviate suffering. Transgenic hemizygous hSOD1G93A male mice expressing high copy number of the mutated allele of human SOD1 gene (Gurney *et al.*, 1994) B6.Cg-Tg(SOD1*G93A)1Gur/J (stock number 004435) were acquired from Jackson Laboratory (Bar Harbor, ME, USA) and bred with non-transgenic C57BL/6J females to produce transgenic (hSOD1G93A) and non-transgenic (control) mice. The genotypes were confirmed by Polymerase Chain Reaction (PCR) on tail biopsies. All animals were maintained in controlled laboratory conditions comprising of 10/14 h light-dark cycle and *ad libitum* access to standard diet and tap water. The hemizygotes exhibit adult-onset neurodegeneration of spinal motor neurons leading to progressive motor deficits & paralysis, similar to ALS patients. The hSOD1G93A mice in our laboratory on C57BL/6J (non-transgenic) background live up to 157.1 ± 9.3 days (https://www.jax.org/strain/004435). Their weight gain is slower than their non-transgenic littermates due to the denervation of muscles and subsequent atrophy (Figure 4).

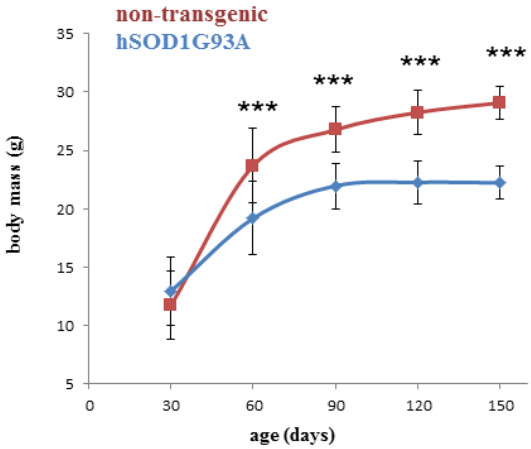

Figure 4. Body mass of hSOD1G93A mice decreases over time when compared to non-transgenic mice. hSOD1G93A mice (n = 181) exhibit weight loss due to muscle atrophy when compared to healthy non-transgenic mice (n = 12). Data for only male mice are shown. Mann Whitney *U* test. ***p ≤ 0.001.

3.2 Mouse primary motor neuron-enriched co-cultures

Spinal cords from 13 day old hSOD1G93A and non-transgenic embryos were extracted for cell isolation. Genotype verification was as suggested by the Jackson Laboratory. Motor neuron-astrocyte primary co-cultures were prepared as previously described (Van Den Bosch *et al.*, 2000; Van Damme *et al.*, 2003) (Figure 5). The mice embryonic ventral spinal cords were dissected and the subsequently extracted motor neurons were seeded on previously prepared glial feeder monolayers.

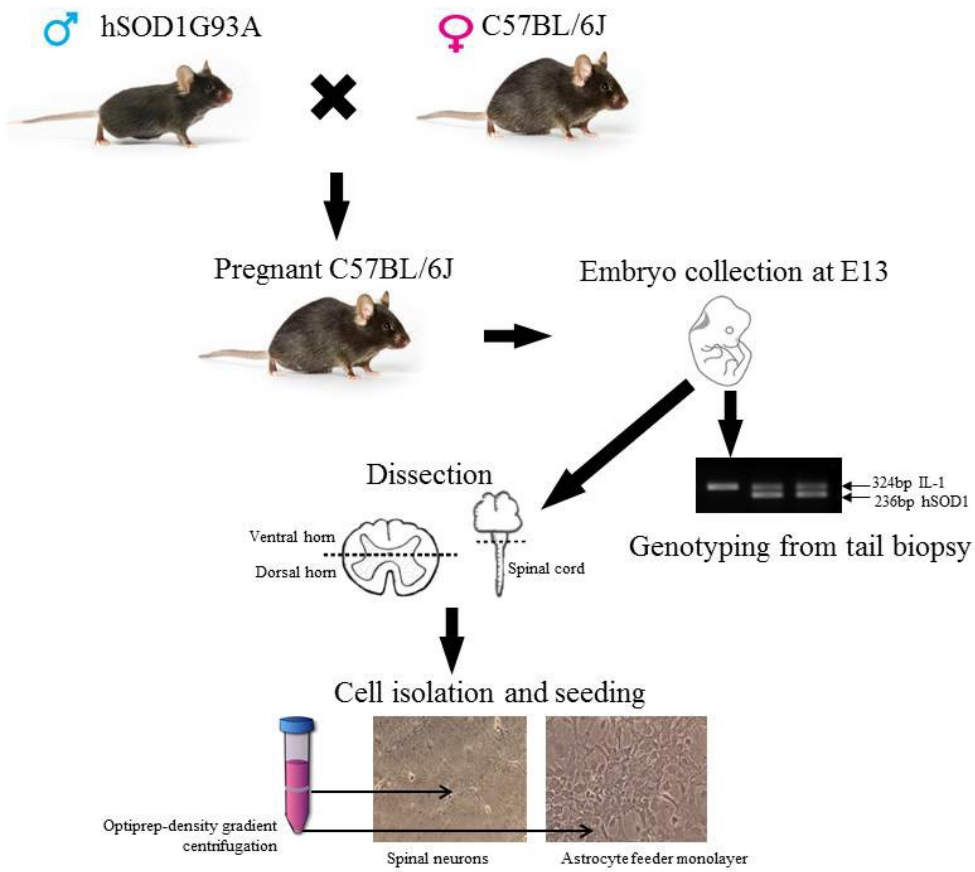

Figure 5. Schematic for primary motor neuron enriched co-culture preparation from mice. Hemizygous hSOD1G3A male is mated with C57BL/6J female. Embryos are collected from the pregnant C57BL/6J mouse at E13 followed by their genotyping and spinal cords isolation. Dissection of ventral horns from embryonic spinal cords is followed by cell dissociation from the tissue and density-gradient centrifugation. Finally, the astrocyte-enriched pellet is seeded to generate feeder monolayers while the spinal neuron fraction is seeded on previously generated feeder astrocyte monolayers. Images of the mice are adapted from Jackson laboratories (https://www.jax.org/).

3.2.1 Genotyping mice embryos

For DNA isolation, 0.2 cm of the tail biopsy from each mouse was treated with 75 µL of alkaline lysis reagent containing 37.5 µL of 25 mM NaOH solution (Riedel-de Haën, Germany) in deionized water and 37.5 µL of 0.2 mM ethylenediaminetetraacetic acid (EDTA, Sigma-Aldrich). After incubating at 95 °C for 30 minutes, the specimens were cooled on ice for 5 minutes. Thereafter, 75 µL of neutralizing agent containing 40 mM tris(hydroxymethyl)-aminomethane hydrochloride (TrisHCl, Roth, Germany) in distilled water was added. 1 µL from each treated sample was subjected to polymerase chain reaction (PCR). For this, 10 µL of MasterMix (5 Prime), 1 µL of each primer (Table 10) (Biomers.net, Germany) and 1 µL of DNA (described above) were added to 10 µL of deionised water in a 0.5 mLeppendorf tube (Eppendorf, Germany). By employing a T3 Thermocycler (Biometra, Germany), PCR was accomplished following the program steps from Table 12. The amplified products were run on 1.5% agarose gel (Sigma-Aldrich, Germany).

3.2.2 Cell culture plates preparation for seeding motor neurons

Prior to seeding motor neurons, autoclaved 12 mm glass coverslips (Marienfeld GmbH) were placed in 24 well NunclonTM Surface plates (Nunc A/S, Denmark) and coated with 150 µL of poly-D-lysine hydrobromide solution (PDL, Sigma-Aldrich). Post 1 hr incubation at 37°C, PDL was removed and the coverslips were washed twice with 500 µL of distilled water followed by addition of 500 µL astrocyte media (Table 1). The plates were kept in the incubator at 37 °C and 5 % CO_2 until seeding.

3.2.3 Generating motor-neuron-enriched co-cultures

Female non-transgenic mice were mated with male hSOD1G93A mice. On day 13 of the pregnancy, the females were sacrificed by cervical dislocation. Each deceased animal was drenched with 70% ethanol (Nordhäuser Ethanol, Germany) to restrict fur contamination. The abdominal pelt was removed and uterus was cut at the mesentery. The uterus and amnions were operated upon to extract the embryos. A piece of the tail from each embryo was excised for genotyping. Subsequently, the ventral spinal cords from hSOD1G93A and non-transgenic embryos were dissected and pooled separately into two 15 mLfalcon tubes containing cold modified HBSS.

To reach the spinal cord, each embryo was pinned with a needle followed by removal of the skin overlying the spinal cord. Dorsal sections of the spinal cord and lumbar regions were excised to extract the ventral horns. Tissue preparation and genotyping of embryos were done by Svetlana Tausch.

The pooled spinal cord sections were washed thrice with 5 mLice-cold modified HBSS and digested with 0.1% trypsin (Gibco, UK, prepared in modified HBSS) for 15 min in a 37 °C waterbath. Subsequently, the tissues were placed on ice and allowed to settle. For trituration, trypsin was discarded and 4 mLof motor neuron medium (Table 1) along with 80 µl ice-cold DNase (AppliChem, Germany) was added. The suspension was agitated for 1-2 minutes to separate the digested tissues. Addition of the medium, also, stopped traces of the trypsin's activity. After the tissues settled, they were slowly triturated using fire-polished glass pipettes to obtain even cell suspension. For isolation of motor-neuron enriched fraction and glial cells, the homogenized solution was subjected to density gradient centrifugation with 6.2% OptiPrep density gradient solution (OptiPrep, Axis-shield Poc AS, Norway) dissolved in L-15 media (Sigma-Aldrich, Germany). Astrocyte feeder monolayers were generated by seeding the glial cells on previously prepared 12-mm PDL-coated coverslips (50,000 cells/coverslip). Glial medium (Table 1), for the first week media change, contained 10% fetal calf serum (FCS, PAN Biotech, Germany). This supports viability and attachment of the astrocytes to the PDL-coated coverslips. Subsequently, FCS was replaced by 10% horse serum (Gibco, UK). The glial cells multiplied till they reached 60-70% confluency after which the cell division was arrested by applying 5 µM arabinofuranosyl cytidine (Calbiochem, Germany) for 24 hr. Spinal motor-neuron enriched fractions were seeded on the glial feeder monolayers (15,000 cells/coverslip for viability assay or immunocytochemistry and 30,000 cells/coverslip for calcium imaging). From the time of seeding the motor neurons, media change was with 500 µl of motor neuron medium (Table 1) per well. On day 13 *in vitro*, the motor neuron co-cultures were used for the experiments.

3.3 Mice cervical sections

3.3.1 Spinal cord isolation

For *ex vivo* studies, both presymptomatic and symptomatic hSOD1G93A animals were used along with age-matched controls (Tables 4 & 5). Mice were first placed in Plexiglas cylindrical chambers and anesthetized until cardiac arrest using isoflurane (Isoflurane-CP, CP-Pharma, Germany). The gas was injected into the sealed chambers using Isoflurane Vapor

19.3 (Drägerwerk AG, Germany). Subsequently, the mice required for cervical section preparation and immunohistochemistry were perfused with PBS (Phosphate Buffered Saline) for 2 minutes followed by a perfusion with 4% ice-cold PFA (paraformaldehyde) to fix the organ tissues. Post perfusion, the mice were decapitated close to their heads. After opening the spinal canals, the cervical regions were severed from the spinal cords and the overhanging nerve roots were trimmed. The spinal cord regions were incubated in ice-cold 4% PFA overnight. Following this, the specimens were immersed in 10% sucrose solution maintained at 4°C and incubated overnight. Finally, they were incubated at 4°C in 30% sucrose till they sunk in the solution. The segments were then frozen in Tissue-Tek® (Sakura, Netherlands) at -20°C. On the other hand, for mRNA expression studies, the mice employed were decapitated after successful anesthesia without perfusion. The entire spinal columns were extracted and stored at -80°C in Tissue Tek.

3.3.2 Spinal cord section preparation

The cervical regions of hSOD1G93A and non-transgenic mice were taken and the CM3050S cryostat (Leica, Germany) maintained at -19°C was employed for slicing. Each spinal cord region was immobilized on the instrument's carrier plate using Tissue-Tek® and sliced to generate 16 µm thick sections. As and when they were sliced, the tissue sections were directly transferred on to SuperFrost Plus® (Thermo-Fisher Scientific™, USA) slides that were pre-warmed to 37°C. Around 10 slices were mounted per slide. Afterwards, the slides were stored at -20°C.

3.4 Protein expression studies

3.4.1 Immunofluorescence of motor-neuron-enriched co-cultures

To distinguish neuronal cell types (motor neurons from non-motor neurons), determine the distribution and quantify expression of IFN-γR1and GluR1 at the embryonic stage, and ascertain dendritic beads formation upon IFN-γ stimulation, immunocytochemistry was performed on primary motor-neuron-enriched co-cultures. The cells from both the genotypes were fixed with 4% PFA for 20 minutes at room temperature. Following double wash with 1X PBS, cells were incubated for 2 hr with 10% normal goat serum (Gibco, UK) that was dissolved in modified PBS (1X PBS + 3% bovine albumin serum (BSA, SERVA) + 0.3% Triton X-100 (Sigma-Aldrich, USA)) at room temperature to prevent unspecific secondary

antibody binding. Primary antibodies were diluted in 2% normal goat serum containing modified PBS. Cells were incubated in primary antibody solution according to the protocols detailed in Table 6. The employed primary antibodies consisted of mouse anti-SMI32 (801701, BioLegend, USA, 1:1000) for motor neuron marker, rabbit anti-βIII-tubulin (T2200, Sigma Aldrich, Germany, 1:250) for general cytoskeleton marker, rabbit anti-MAP-2 (ab32454, Abcam, UK, 1:200) rabbit polyclonal anti-IFN-γR1 (sc-702, Santa Cruz Biotechnology Inc., CA, USA, 1:200), and rabbit anti-GluR1 (ab31232, Abcam, UK, 1:200). Post antibody incubation, the cells were washed twice with 1X PBS and incubated with the appropriate secondary antibody dissolved in modified PBS containing 10% NGS (Table 6). Thereafter, a double wash with PBS was followed by staining of all the nuclei with 4', 6-diamidino-2-phenylindole (DAPI, Sigma, USA) for 5 minutes. The last step involved washing out of DAPI with 1X PBS and mounting of the coverslips with Fluoromount-G (SouthernBiotech, UK).

3.4.2 Immunohistochemistry of spinal cord sections

Slides containing the spinal cord sections stored in -20°C were transferred to glass cuvettes and left to dry in a cabinet maintained at 37°C for 30 minutes. They were then incubated with 1% SDS (Sodiumdodecyl sulfate) at room temperature for 5 minutes for antigen retrieval. Subsequently, the spinal cord sections were rinsed twice with 1X PBS for 5 and 10 minutes. 2 hr incubation with 10% normal goat serum was carried out for blocking at room temperature. Tissue slices were stained using primary antibodies of rabbit anti-IFN-γR1(sc-702, Santa Cruz Biotechnology Inc., CA, USA, 1:200), rabbit anti-GluR1 (ab31232, Abcam, UK, 1:200), monoclonal rabbit anti-phospho-Stat1(Tyr701) antibody (Cell Signaling Technology, Danvers, MA, USA, 1:250), or rabbit anti-JAK1 (H-106, Santa Cruz, 1:250) along with mouse anti-SMI32 (1:1000) that were dissolved in 2% NGS. The antibody solution was added onto the slides and covered with Parafilm® (Bemis, USA). The slides were carefully transferred to a wet chamber and kept for 48 hours at 4°C. Subsequently, the slides were washed in 1X PBS thrice for 15 minutes each time. Secondary antibodies Alexa 488 goat anti-rabbit and Alexa 594 goat anti-mouse diluted in 10% NGS were added. Incubation was for 1 hr at room temperature, which was followed by 1X PBS wash twice.

Thereafter, the slices were stained with DAPI for nuclei identification by immersing the slides in the solution for 5 minutes. Finally, the sections were thoroughly rinsed with 1X PBS and

mounted with Fluoromount-G® (SouthernBiotech, USA). The specimens were stored at 4°C in the dark until analyses were performed.

3.4.3 Quantification of immunofluorescence signal

For the motor-neuron co-cultures, immunofluorescence signals representing protein expression levels of IFN-©R1and GluR1 were quantified in non-transgenic and hSOD1G93A motor neurons. At least 5 neurons from each coverslip out of a set of 3 coverslips per motor neuron culture preparation were imaged. This was repeated for at least 3 different cell culture preparations (1 n = 1 motor neuron). For *ex vivo* expression studies, at least 15 cells from the anterior horns of 3 spinal cord sections (cervical) of one animal were imaged (1 n = 1 neuron). Immunofluorescence signals of IFN-γR1, GluR1, JAK1, and phosphorylated STAT1 were quantified. High resolution volumetric images of the stained motor neurons were generated by acquiring sequential optical sections (z-stacks) in high magnification (63X oil immersion) through confocal laser scanning microscopy (LSM 710, Zeiss, Germany) having constant settings (PMT voltage, scan speed, pinhole etc.). For image processing, ZEN 2012 software (Zeiss, Germany) was employed. Integrated fluorescence density and mean fluorescence were measured with the "z-project" plugin of the Fiji Is Just ImageJ software 2014 (Fiji, open source software based on ImageJ modified by BioVoxxel, Mutterstadt, Germany). To measure protein expression, the corrected total cell fluorescence (CTCF) was computed using the formula: CTCF = Integrated density of selection – (Area of the selection X Mean fluorescence of background readings) (Gavet & Pines, 2010). CTCF data from single motor neurons belonging to the same genotype were pooled (1 cell = 1 n).

3.5 mRNA expression studies

3.5.1 Sample preparation from motor neuron co-cultures and spinal cords

qPCR was performed in collaboration with Madlen Gunther to determine mRNA levels of targets of interest (IFN-γR1, GluR1, JAK1, Stat1, PKA isoforms). For mRNA measurements in embryonic system, cells from three coverslips of each motor neuron-enriched co-culture preparation were pooled as one sample (1 preparation = 1 n) after adding 100 µl QIAzol lysis reagent (Qiagen, USA) to each well.

For *ex-vivo* expression studies, the spinal columns were transferred to liquid nitrogen vessels and 1µl QIAzol Lysis Reagent was added to each specimen. The tissues were homogenized in Ultrathorax (Miccra, Germany) for 10-20 seconds.

3.5.2 RNA isolation

Total RNA from primary cells and spinal cord tissue were extracted by employing the phenol/chloroform extraction method. The samples, after lysis, were allowed to rest for 5 minutes at room temperature, after which they were dissolved in 200 µL of chloroform (Sigma-Aldrich, USA). After vigorously shaking by hand for 15 s and incubating for 3 minutes at room temperature, the samples were centrifuged at 12000xg for 15 minutes at 4°C. Subsequently, the liquid phase of the solution from the surface was extracted for each sample and collected in a new tube. The RNA in the collected aqueous phase was then precipitated with 1.1-fold volume of isopropranol (Sigma-Aldrich, USA) and 0.16-fold volume of 2M sodium acetate (Sigma-Aldrich, USA) at pH 4. After dissolving, the RNA containing solution was maintained at -20°C overnight. Subsequently, the suspension was again centrifuged at 12000xg for 15 minutes at 4°C. The supernatant was discarded and the pellet containing RNA was washed with 1 mLof 75% ethanol, dissolved using a vortex shaker, and centrifuged at 7500xg for 10 minutes at 4°C. Subsequently, the pellet was again washed with the same amount of ethanol after removing the supernatant. The pellet was spun down and the rest of the liquid was then pipetted out. Finally, after air-drying for 5-10 minutes, the pellet was dissolved in 40 µL of DEPC-H_2O (Gibco, UK) by pipetting up and down for 5 minutes at 65°C. The RNA was stored at -80°C after determining its concentration using NanoDrop 2000 (Peqlab Biotechnologies,Germany).

3.5.3 cDNA synthesis

To synthesize cDNA, total RNA (500ng) was transcribed using the Revert Aid First strand cDNA synthesis kit (ThermoFisher Scientific, USA). Briefly, 0.5µL random hexamer primer, 0.6µL oligo (dT) 18 primer, and 5µL RNA were mixed in a 0.2µL reaction tube at 4°C. Subsequently, the tube was subjected to 65°C for 5 minutes followed by incubation for at least 2 minutes at 4°C. Based on the number of samples, the master mix was made with 2µL of 5x reaction buffer, 1µL of 10mM deoxynucleoside triphosphates (dNTPs), 0.5µL of

RNAse inhibitor and 0.5µL of reverse transcriptase. The master mix was then added to the pre-incubated RNA sample followed by pipetting up and down to mix the solutions. This final mixture was then subjected to a thermal cycling program (25°C for 5 minutes, 42°C for 60 minutes, 70°C for 5 minutes). The generated cDNA was diluted with distilled water at a 1:10 ratio to obtain a final concentration of 5ng/µL.

3.5.4 qPCR reaction

qPCR was done with SYBR Green III Master Mix (Agilent Technologies, USA) as formerly described (Jaenisch *et al.*, 2016). 10µL of 10X SYBR Green III Master Mix and 5µL of 2µM Primermix (Biomers.net, Germany) were mixed in a reaction tube. The mRNAs of target interests were normalized to a housekeeping gene -- hydroxymethylbilane synthase (hmbs) or Glyceraldehyde 3-phosphate dehydrogenase (GAPDH). Primers used for qPCR are listed in Table 9.

To 5µL of previously obtained cDNA, 15µL of the SYBR Green reaction mixture was added followed by running it in Corbett Rotor Gene 6000 PCR cycler (Corbett Life Science Pty. Ltd., Australia) using the following thermal cycling program: polymerase activation at 95°C for 3 minutes, 40 amplification cycles (95°C for 10 s, 60°C for 15 s) followed by melting curve measurement. The relative mRNA expression of target proteins for each hSOD1G93A sample was calculated to the mean value from non-transgenic sample by applying Pfaffl equation (Pfaffl, 2001). Apart from cycle threshold (Ct), the qPCR efficiency (E) and melting temperature of the product were supplied by the commercially available software of the PCR cycler. While the Ct value suggests the number of cycles required for the product's fluorescence signal to cross the set threshold, availability of the melting temperature ensures that the product is specifically amplified. The Pfaffl equation that was employed for calculations is given below:

$$R = \{(E_{\text{target sequence}})^{\text{Ct target control} - \text{Ct target sample}}\} / \{(E_{\text{reference sequence}})^{\text{Ct reference control} - \text{Ct reference sample}}\}$$

Subsequently, the geometric mean of R for all the animal groups was determined.

3.6 Functional tests for IFN-γ

3.6.1 Staining and visualizing dendritic beads *in vitro*

At the outset, for functional studies, it was appropriate to verify if IFN-γ exerts visible effects that could be visualized as dendritic beads in the motor neurons from the cell culture system employed in this study. To determine this, day 13 *in vitro* primary motor neuron-enriched cultures of both hSOD1G93A and non-transgenic genotypes were treated with 100 ng/mLof recombinant IFN-γ for 12 hr. Subsequently, the co-cultures were stained for MAP-2 and SMI32 and observed under 20X magnification of a fluorescence microscope (LSM 710, Zeiss, Germany).

3.6.2 Cell survival study on primary motor-neuron-enriched co-cultures

To determine effect of IFN-γ on motor neuron survival, we tested the cytokine's independent impact as well as its role in AMPAR-mediated excitotoxicity. In this study, the potent AMPAR receptor agonist kainate was used to induce excitotoxicity. Thus, the treatment strategy involved application of recombinant IFN-γ alone or in combination with kainate. On day 13 *in vitro*, motor neuron enriched cultures were treated for 12 hr and 24 hr at 37^{o}C in a humidified CO_2 incubator with (Table 13): 100 μM kainate (Abcam, UK) and/or 100 ng/mLIFN-γ (R & D Systems, USA). The cells were fixed with 4 % PFA and blocked with 10% normal goat serum in 1% BSA. Following this, they were stained with the neuronal general cytoskeleton marker βIII-tubulin and motor neuron marker SMI32. The numbers of βIII-tubulin-positive neurons representing all neurons and βIII-tubulin+SMI32-positive neurons representing the motor neuron kind were counted in characteristic areas per coverslip by an investigator blinded to the experimental conditions. All the coverslips were examined under a fluorescence microscope (Axioplan 2 imaging, Zeiss, Germany) at 20X magnification in atleast 3 independent repeats. The numbers were compared to native (untreated) controls.

3.6.3 Single cell cytosolic calcium measurements

Cytosolic calcium (Ca^{2+}) measurement was by means of Fura-2 single cell imaging. Motor neuron enriched co-cultures were loaded with 5-10 μM of the membrane permeable ester form of the high-affinity ratiometric fluorescent dye Fura-2AM (Sigma Aldrich, Germany) for 25 minutes at 37°C. After dye de-esterification at room temperature, motor neuron-enriched

culture containing coverslip was mounted onto the stage of an upright microscope (Nikon Microscope Eclipse FN1, Tokyo, Japan) that was constantly perfused with a standard extracellular solution containing (in mM): 3.2 $CaCl_2$, 129.1 NaCl, 11.6 HEPES, 5.9 KCl, 1.2 $MgCl_2$, and 11.5 glucose and pH adjusted to 7.4 with NaOH (Table 14). Cell visualization was by using a water immersion objective (NIR Apo, 40X/0.80 W, DIC N2, ∞/0, WD 3.5) (Nikon, Tokyo, Japan) and exciting Fura-2 at 350 and 380 nm wavelengths (Polychrome V, TillPhotonics, Gräfelfing, Germany). Emission light transmitted through the dichroic mirror (DCLP410) and emission filter (LP440, both obtained from TillPhotonics) was collected by a cooled CCD camera (iXON$_{EM}$+, ANDOR™, UK) as described previously (Grosskreutz et al., 2007). Ratiometric fluorescent images were captured using the Till Vision Imaging System (TillPhotonics, Gräfelfing, Germany). To determine the direct effect of IFN-γ on intracellular Ca^{2+} at single-cell level, varying doses (100 ng/mL, 200 ng/mL, and 500 ng/mL) of IFN-γ were directly applied for durations ranging from 2 s at 30 s intervals to 2 hr without intervals. Also, cells were pre-incubated with 100 ng/mLof IFN-γ for 30 or 60 minutes and subjected to kainate for 2 s at 30 s intervals. The calcium measurements were done both in the presence and absence of other channel blockers, namely 200 µM verapamil (Sigma-Aldrich, Germany) and 0.5µM tetrodotoxin (Biotrend, Germany). While verapamil blocks the voltage-gated calcium channels, tetrodotoxin selectively blocks voltage-gated sodium channels. In the case of using channel blockers, the extracellular solution used to superfuse the cells, also, contained these two substances during the entire measurement course.

3.7 Statistics

The statistical analyses were performed using GraphPad Prism Version 5.00 for Windows. Data are given as mean ± SEM except for that of survival study in which the data are provided as mean ± SD. Scatter plots, box plots (min, max, quartile) and bar charts have been used for data representations. All the analyzed data were tested for normality and equal variances. For non-parametric data, Mann-Whitney test was employed to compare two groups. ANOVA with Bonferroni's correction as post-hoc test was used for multiple comparisons. The threshold for statistical significance was considered at $p < 0.05$.

3.8 Buffers, media, and other consumables

3.8.1 Media preparation and materials for motor-neuron co-cultures

Media	Components	Concentration
Astrocyte medium	DMEM / Ham's F-12 Medium	Base
	FCS or horse serum	10%
	Penicillin-Streptomycin	1%
Motor neuron medium	Neurobasal Medium	Base
	B27 Neuromix (50x)	2%
	BDNF	2 ng/mL
	Horse serum	2%
	L-Glutamine	1 mM
	N2 Supplement (100x)	0,2%
	Penicillin-Streptomycin	1%
Modified HBSS	HBSS	Base
	HEPES	1 M
	Penicillin-Streptomycin	1%
PBS	KCl	2.7 mM
	KH_2PO_4	1.8 mM
	NaCl	137 mM
	$NaHPO_4$	10 mM

Table 1. Media and buffers used for cell culture and immunocytochemistry. HBSS: Hank's Balanced Salt Solution, KCl: Potassium Chloride, KH_2PO4: Potassium Dihydrogen Phosphate, NaCl: Sodium Chloride, PBS: Phosphate-Buffered Saline. FCS: Fetal Calf Serum, DMEM: Dulbecco's Modified Eagle Medium; BDNF: Brain-derived neurotrophic factor, HEPES: (4-(2-hydroxyethyl)-1-piperazineethanesulfonic acid.

Substances	**Manufacturer**
1-β-Arabinofuranosylcytosine (AraC)	Calbiochem, Germany
4-(2-hydroxyethyl)-1-piperazineethanesulfonic acid (HEPES)	Roth, Germany
Absolute ethanol for analysis	Merck, Germany
Acetic acid	Roth, Germany
B27 NeuroMix (50x)	Gibco, UK
Bovine serum albumin (BSA)	SERVA, Germany
DNase I	AppliChem, USA
Dulbecco's modified Eagle's medium (DMEM) / Ham's F-12 Medium (1:1) without L-glutamine	Gibco, UK
Fetal calf serum (FCS)	PAN Biotech, Germany
Ham's F-12 Medium (1:1) without L-Glutamine	Gibco, UK
Hank's balanced salt solution (HBSS)	Gibco, UK
HCl	Sigma, USA
Horse serum	Gibco, UK
KCl	Merck, Germany
L-15 Medium Leibovitz without L-glutamine	Sigma, Germany
L-Glutamine (200mM 100x)	Gibco, UK
$NaHPO_4$	Roth, Germany
N2 supplement (100x)	Gibco, UK
NaCl	Roth, Germany
Neurobasal medium without L-Glutamine	Gibco, UK
Normal goat serum (NGS)	Gibco, UK
OptiPrepTM	AXIS-SHIELD, Norway
Penicillin-Streptomycin	Gibco, UK
Poly-D-lysine hydrobromide	Sigma Aldrich, USA
Recombinant human brain-derived neurotrophic factor (BDNF)	PeproTech, USA
Sodiumdodecylsulfate (SDS)	SERVA, Germany
Sodium hydroxide (NaOH)	Sigma, Germany
Tris (hydroxymethyl) aminoethane hydrochloride (TrisHCl)	Roth, Germany
Trypsin	Gibco, UK
Water for injection	Fresenius Kabi, GER

Table 2. Ingredients for cell culture preparation.

Consumable	Properties	Manufacturer
24-well plates		Greiner Bio-One, Germany
Biosphere filter tips	Different sizes	Sarstedt, Germany
Coverslips	Diameter = 12mm	Marienfeld GmbH & Co KG, Germany
Eppendorf tubes	0.5ml, 1.5ml, 2ml, 5ml	Eppendorf, Germany
Falcon tubes	15ml; 50ml	Greiner Bio-One, Germany
Nunclon Surface plates		Nunc A/S, Denmark
Pasteur pipettes	230mm	Assistent, Germany
Transfer pipettes		Sarstedt, Germany

Table 3. Laboratory consumables for cell culture preparation.

3.8.2 Animals for *ex-vivo* studies

	hSOD1G93A	C57BL/6J
Presymptomatic group	3 (9 - 9.1 weeks old)	3 (8.1 weeks old)
Symptomatic group	3 (19.6 - 20.6 weeks old)	3 (21.3 weeks old)

Table 4. Number of animals used per group for protein expression studies (CTCF evaluation)

	hSOD1G93A	C57BL/6J
Presymptomatic group	6 (9.2 – 10.2 weeks old)	3 (9.8 weeks old)
Symptomatic group	7 (19 - 21.3 weeks old)	5 (17.7-21 weeks old)

Table 5. Number of animals used per group for relative mRNA expression studies

3.8.3 Ingredients for immunofluorescence staining protocols

Target of interest	Primary antibody	Dilution, temperature, & incubation period	Secondary antibody	Dilution, temperature, & incubation period
βIII tubulin	Rabbit anti-β-tubulin III, Sigma Aldrich	1:250, RT, 1 hr	Alexa 488 goat anti-rabbit, Invitrogen; USA	1:250, RT, 1 hr
GluR1	Rabbit anti-GluR1, Abcam	1:100, 4°C, overnight	Alexa 488 goat anti-rabbit, Invitrogen; USA	1:250, RT, 1hr
IFN-γR1	Rabbit anti-IFN-©R1 , Santa	1:200, 4°C, overnight	Alexa 488 goat anti-rabbit, Invitrogen; USA	1:250, RT, 1hr
JAK1	Rabbit anti-JAK1, Santa Cruz	1:250, 4°C, overnight	Alexa 488 goat anti-rabbit, Invitrogen; USA	1:250, RT, 1hr
MAP-2	Rabbit anti-MAP2, Abcam	1:200, RT, 1 hr	Alexa 488 goat anti-rabbit, Invitrogen; USA	1:250, RT, 1hr
pSTAT1	Rabbit anti-phosphoStat1(Tyr701), Cell Signaling Technology	1:250, 4°C, overnight	Alexa 488 goat anti-rabbit, Invitrogen; USA	1:250, RT, 1hr
SMI32	Mouse anti-SMI32, BioLegend, USA,	1:1000, 4°C, overnight	Alexa 594 goat anti-mouse, Invitrogen; USA	1:250, RT, 1hr

Table 6. Primary and secondary antibody list alongwith protocols for staining. GluR1: Glutamate Receptor 1, IFN-γR1: Interferon-Gamma Receptor 1, JAK1: Janus Kinase 1, MAP-2: Microtubule-Associated Protein 2, pSTAT1: Phosphorylated STAT1(Signal Transducer and Activator of Transcription 1), SMI32: Motor neuron neurofilament marker

Solution/Buffer	Constitution
Modified Phosphate Buffer Saline (PBS)	3% Bovine Serum Albumin (BSA) and 0.3% Triton-X-100 in 1X PBS
Sodiumdodecyl Sulfate (SDS) solution	1% SDS in 1X PBS
Blocking and secondary antibody solution	10% Normal Goat Serum in modified PBS
Primary antibody solution	2% Normal Goat Serum in modified PBS

Table 7. Buffers and solutions used for immunostaining

3.8.4 Materials for PCR and qPCR

Commercial kit/substance	Constituents	Manufacturer, Location
Revert aid first strand cDNA synthesis kit	Oligo (dT) primer Random hexamer primer 5x Reaction buffer Deoxynucleotriphosphates (dNTPs) RNAse inhibitor (20U/µl) Reverse transcriptase (200U/µl)	Thermo Fisher Scientific, USA
10X SYBR Green III Master Mix		Agilent Technologies, USA

Table 8. Commercial kit and other relevant materials for qPCR.

Gene	Primer sequences	Product Size
Gapdh	Fwd: CAACAGCAACTCCCACTCTTC Rev: GGTCCAGGGTTTCTTACTCCTT	164 bp
hmbs	Fwd: GAAATCATTGCTATGTCCACCA Rev: GCGTTTTCTAGCTCCTTGGTAA	98 bp
GRIA1	Fwd: CAAATCCCGTAGCGAGTCGA Rev: TCTGCCATTCTCTCCACTGC	144 bp
IFN-©R1	Fwd: GGTGGTTGCTCCTCTTACCG Rev: ACCACAGAGAGCAAGGACTTAG	120 bp
JAK1	Fwd: CTGAGGTATTGGGTGGCCAG Rev: CTTATGTTGTCCGTGCGCAG	154 bp
Prkaca	Fwd: TTTGCCAAGCGTGTGAAAGG Rev: GTAACCAGCAGCCATCTCGT	147 bp
Prkacb	Fwd: TGCAGCCCAGATTGTGCTAA Rev: ATGTCCATGTCCTGCCCTTG	155 bp
Stat1	Fwd: CTGCTGTGCCTCTGGAATGA Rev: TGAATGTGATGGCCCCTTCC	139 bp

Table 9. Primers for qPCR. GRIA1: Glutamate Receptor 1, IFN-©R1: Interferon-Gamma Receptor 1, JAK1: Janus Kinase 1, Prkaca: Protein Kinase A catalytic subunit A, Prkacb: Protein Kinase A catalytic subunit B, Stat1: Signal Transducer and Activator of Transcription 1

Primer name	Primer sequence
Internal control (oIMR7338)	Fwd: CTAGGCCACAGAATTGAAAGATCT
Internal control (oIMR7339)	Rev: GTAGGTGGAAATTCTAGCATCATCC
Transgenic SOD1 (oIMR0113)	Fwd: CATCAGCCCTAATCCATCTGA
Transgenic SOD1 (oIMR0114)	Rev: CGCGACTAACAATCAAAGTGA

Table 10. Primers for genotyping mouse embryos.

Material	Constituents	Company
PCR Master Mix	*Taq* DNA Polymerase (62.5U/mL), 125mM KCl, 0.25% Igepal®-CA360, 500∝M of each dNTP, 75mM Tris-HCl pH 8.3, 3.75mM $Mg(OAc)_2$, and stabilizers	5Prime, Germany
Primer Mix		Biomers.net, Germany

Table 11. Materials for PCR. KCl: Potassium Chloride, dNTP: deoxynucleotriphosphates, $Mg(OAc)_2$: Magnesium acetate

Cycle Step	Temperature	Time period	No. of cycles
Initial Denaturation	95°C	3 minutes	1
Denaturation Annealing Elongation	95°C 60°C 72°C	30 seconds 30 seconds 45 seconds	35 times in sequence
Final denaturation	72°C	2 minutes	1

Table 12. PCR thermal cycling program for genotyping of hSOD1G93A mice

3.8.5 Chemicals used for cell survival study and calcium measurements

Chemical	Stock Concentration	Solvent	Manufacturer
Kainate	10mM	Purified water	Abcam, UK
IFN-γ	100µg/ml	1X PBS with 0.2% BSA	R&D Systems, USA
Tetrodotoxin	1mM	Purified water	Biotrend, Germany
Verapamil	20mM	DMSO:Purified water (1 : 4)	Sigma Aldrich, Germany
Fura-2AM	2mM	DMSO	Sigma Aldrich, USA

Table 13. Substances used for cell survival study and calcium imaging.

Constituent	Concentration	Company
$CaCl_2$	3.2 mM	Roth, Germany
HEPES	11.6 mM	Roth, Germany
KCl	5.9 mM	Roth, Germany
$MgCl_2$	1.2 mM	Roth, Germany
NaCl	129.1 mM	Merck, Germany

Table 14. Composition of extracellular solution used for calcium imaging. $CaCl_2$: Calcium Chloride, HEPES: 4-(2-hydroxyethyl)-1-piperazineethanesulfonic acid, KCl: potassium chloride, $MgCl_2$: magnesium chloride, NaCl: sodium chloride

3.8.6 Hardware list

Instrument	Company, Location
Centrifuge 5415 R	Eppendorf, Germany
Corbett Rotor Gene 6000 PCR cycler	Corbett Life Science Pty. Ltd., Australia
Cryostat CM3050S	Leica, Germany
D-6450 Type T6120 Drying cabinet	Heraeus, Germany
Isoflurane Vapor 19.3	Drägerwerk, Germany
Laser scanning microscope 710 (LSM 710)	Carl Zeiss, Germany
Miccra D1	Miccra, Germany
Nanodrop 2000	Peqlab Technologies, Germany
T3 Thermocycler	Biometra, Germany

Table 15. List of instruments used for the study

3.8.7 Software list

Software Name	Organization
BLAST	NCBI
FIJI/Image J	BioVoxxel, Germany
GraphPad Prism	GraphPad Software Inc., USA
Mendeley	Elsevier
Microsoft Office Word 2003 & 2010	Microsoft, USA
Till Vision	Till Photonics, Germany
Zen 2012	Carl Zeiss, Germany

Table 16. List of software employed for the study

4. RESULTS

4.1 *In vitro* expression and function studies

4.1.1 Treating primary motor-neuron co-cultures with recombinant IFN-γ induced dendritic bead formation

To determine if IFN-γ independently exerts any conspicuous effects, the primary motor neuron enriched co-cultures were treated with 100 ng/mLof recombinant IFN-γ for 12 hr. Upon staining for MAP-2 and observing under 20X magnification, dendritic beads were clearly visible in both hSOD1G93A and non-transgenic cultures. Irrespective of the genotype, IFN-γ induced dendritic beads in the motor neurons (Figure 6). To investigate the extent of damage, percentage of dendritic bead bearing motor neurons out of total number of motor neurons were determined in 3 independent repeats. Again, all the motor neurons exhibited beading in both the genotypes.

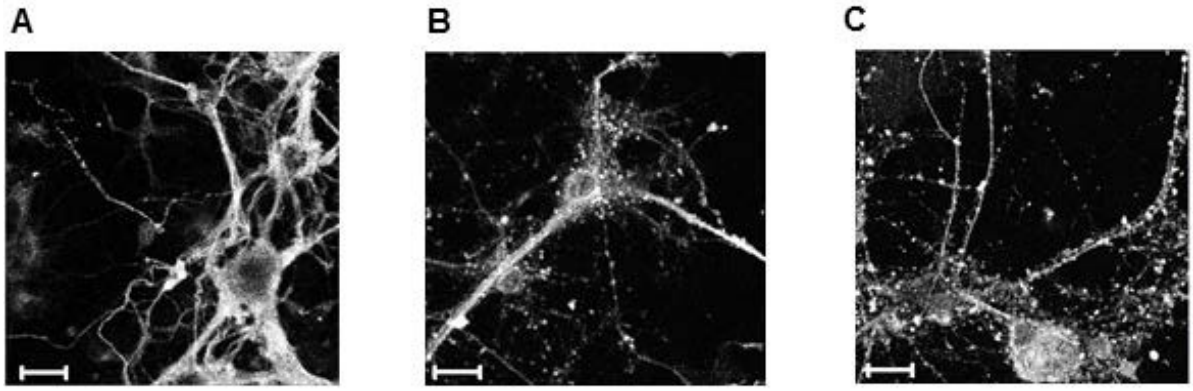

Figure 6. IFN-γ independently induces damage in spinal motor neurons that are visualized as dendritic beads under 20X magnification. Scale bar = 20 μm (A) Untreated non-transgenic spinal motor neurons showing smooth dendrites after MAP-2 staining. IFN-γ independently induces dendritic beads in both (B) non-transgenic and (C) hSOD1G93A motor neurons.

4.1.2 Direct application of IFN-γ maintains AMPAR mediated excitotoxicity in motor neurons

With visible structural changes observation in motor neurons upon IFN-γ application, the next objective was to determine this cytokine's effects on motor neuron survival.

As kainate, a potent AMPAR agonist, and IFN-γ are capable of triggering calcium influx unaided, they were applied independently or in combination to examine excitotoxicity in motor neurons. E13 motor-neuron-enriched co-cultures were treated for 12 hr or 24 hr with 100μM kainate and 100ng/mLIFN-γ in combination as well as alone. Untreated culture wells served as controls. Thus, there were 4 groups for each round of experiment for each genotype: Untreated, kainate treated, IFN-γ treated, and kainate + IFN-γ treated. Post incubation, the surviving neurons were stained for β-III tubulin and SMI32. They were then counted under 20X magnification by an investigator blinded to the treatment conditions (Figure 7).

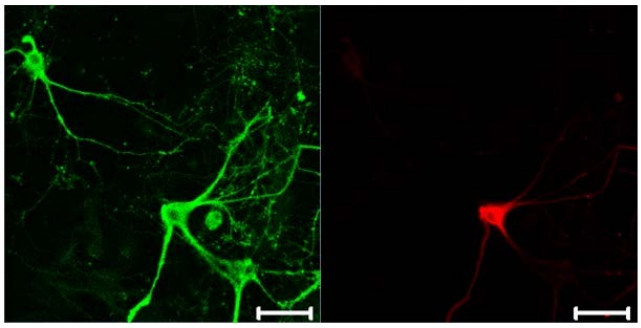

Figure 7. Representative image for neuron counting in survival study. Scale bar = 50 μm. For each coverslip, total number of neurons identified by β-III tubulin staining were counted under a fluorescence microscope in the green channel followed by a switch to the red channel to count the number of motor neurons alone that were identified by SMI32 staining.

As seen with cortical neurons *in vitro* in a previous study (Mizuno *et al.*, 2008), regardless of the incubation time, IFN-γ independently did not exert lethal effect on non-transgenic or hSOD1G93A motor neurons when compared to the untreated group (Figure 8). However, stimulation with both kainate and IFN-γ also did not enhance excitotoxic effect of kainate in non-transgenic (n = 9) and hSOD1G93A (n = 12) motor neurons after 12 hr incubation (Figure 8A). Similar results were seen post 24 hr incubation in hSOD1G93A (n = 9) and non-transgenic (n = 9) motor neurons (Figure 8B). This observation contrasted with the one in the cortical neuron study wherein IFN-γ was shown to promote excitotoxic death in cortical

neurons (Mizuno *et al.*, 2008). Thus, AMPAR mediated excitotoxicity in spinal motor neurons *in vitro* appears to be unaltered by the presence of IFN-γ.

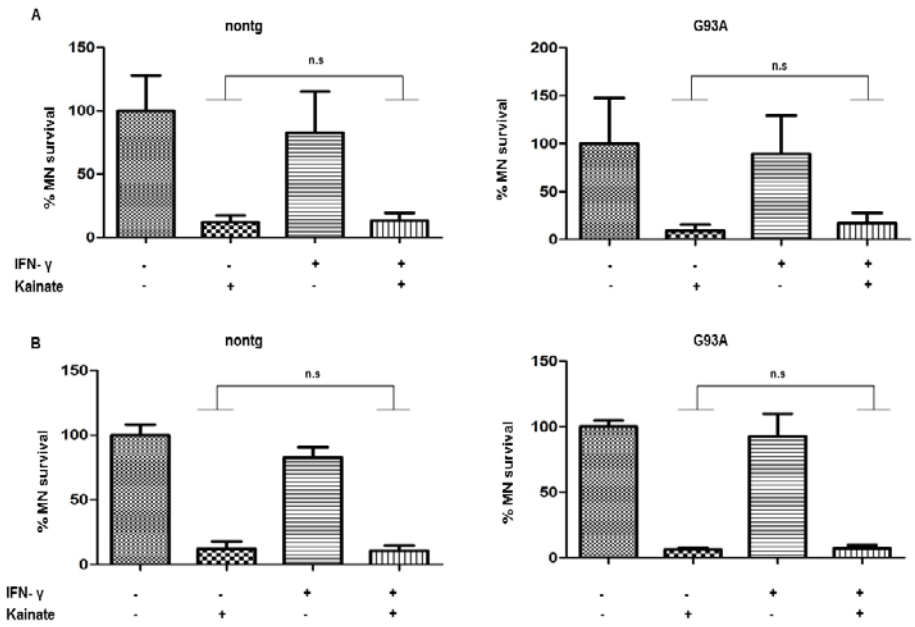

Figure 8. Kainate-induced AMPAR excitotoxicity unaffected by IFN-γ. (A) Both non-transgenic (n = 9) and hSOD1G93A (n = 12) motor neuron co-cultures were treated with combination of IFN-γ and kainate or either of the agents for 12 hr. Kainate treatment induces strong neuronal death and IFN-γ does not appear to add excitotoxic insult (B) A 24 hr treatment yields similar decrease in motor neuron survival post kainate treatment, independent of IFN-γ in both non-transgenic (n = 9) and hSOD1G93A (n = 9) motor neurons. Each column indicates mean ± SD. One-way ANOVA with Bonferroni correction.

4.1.3 Irrespective of the genotype, IFN-γ triggers weak cytosolic calcium signals in single motor neurons *in vitro*

To examine the effects of IFN-γ alone on the cytosolic calcium levels of hSOD1G93A motor neurons as against non-transgenic motor neurons at single cell level, calcium measurements were performed. The process began with attempting to elicit calcium responses by applying low doses (100ng/mL, 200ng/mL) of IFN-γ in the presence of other channel blockers, verapamil and tetrodotoxin (TTX), for short time: 2s at 100s intervals directly to the primary motor neuron cultures. This stimulation protocol is established in our group for AMPAR

stimulation with kainate. The stimulation hardly yielded significant responses. The neurons that did respond gave out weak signals at random time points for both the genotypes.

Reckoning that the dose was probably low for a sufficient response, the concentration was increased by at least 5 times and 500 ng/mLof IFN-γ was applied in the presence of other channel blockers, verapamil and TTX. Regardless of hSOD1G93A presence, both short-term (2 s exposure at 100 s intervals) and long-term (1 min to 1 hr) exposure mostly yielded no/inconsistent weak responses. The direct application protocols of high and low doses were, also, tested in the absence of the channel blockers and the results were similar as the previous ones in both non-transgenic and hSOD1G93A motor neuron cultures. Next, the primary motor neuron co-cultures were pre-incubated with IFN-γ for 30 or 60 minutes to sensitize the IFN-γR1, which was followed by application of our established kainate stimulation protocol. The objective was to stimulate AMPARs after possible sensitizing of the IFN-©R with its cytokine. The responses were typical of that from sole kainate application, irrespective of the genotype. Moreover, cycles of direct IFN-γ application for 2s followed by 100s washout and a 2s kainate pulse also resulted in responses comparable to sole kainate application. Due to lack of consistent, measurable calcium responses from IFN-γ application (both direct and indirect), statistical analyses weren't performed. To determine if there was any difference in the number of neurons between non-transgenic and hSOD1G93A that responded to all the tested protocols, we compared the percentages of responding neurons of both the genotypes. The percentages were very similar (Figure 9C). Moreover, we pooled calcium measurements from one of the tested protocols of direct IFN-γ application with 3 independent repeats to get collective representative images of inconsistent weak responses from non-transgenic (n =16) (Figure 9A) and hSOD1G93A (n = 13) (Figure 9B) neurons.

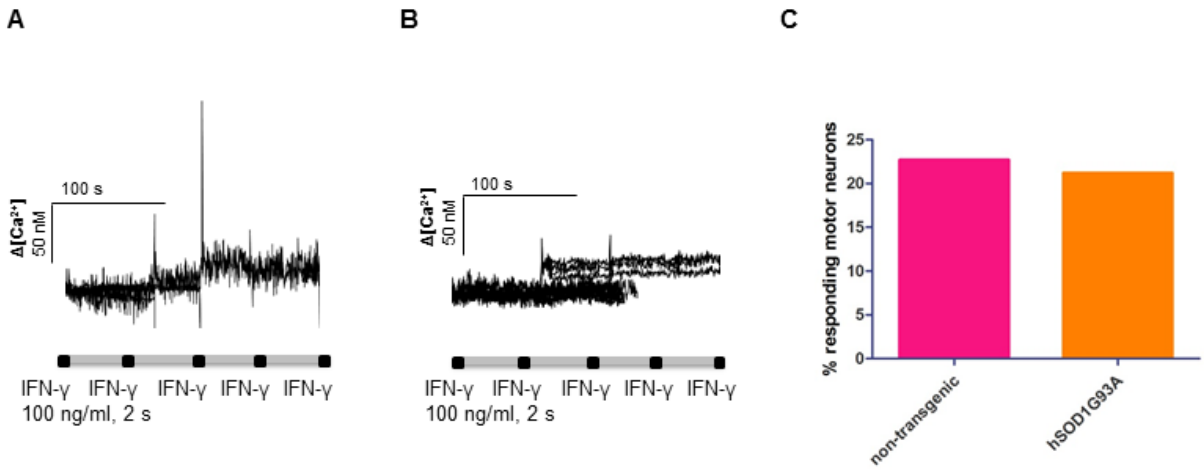

Figure 9. Evaluation of cytosolic calcium levels after direct application of IFN-γ. Representative recording of cytosolic calcium measurement in (A) hSOD1G93A (n = 13) motor neurons and (B) non-transgenic (n = 16) motor neurons. IFN-γ was directly applied for 2 s at 100 s intervals in the presence of channel blockers verapamil and tetradotoxin. Similarly, measurements were carried out under different experimental conditions. All of them yielded weak, inconsistent responses. (C) Counting the percentage of neurons that responded from all the experimental conditions yielded similar numbers in both non-transgenic and hSOD1G93A genotypes.

Table 17. Calcium traces from IFN-γ stimulation by direct application.

PROTOCOL	OBSERVATION	REPEATS
A. 100 ng/mLIFN-γ in the presence of Verapamil (VP) and Tetrodotoxin (TTX) for 2 seconds at 100 second interval	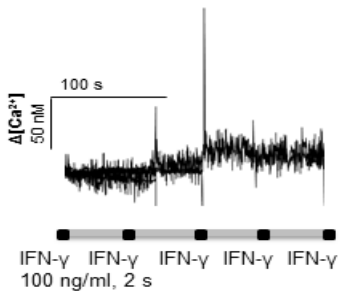	3 different preparations
B. 200 ng/mLIFN-γ in the presence of Verapamil (VP) and Tetrodotoxin (TTX) for 2 seconds at 100 second interval	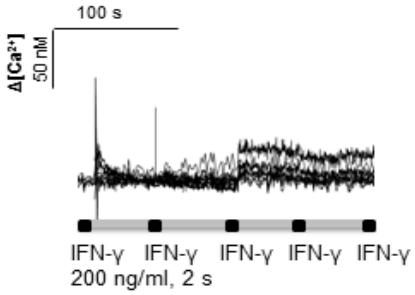	2 different preparations
C. 100 ng/mLIFN-γ in the absence of Verapamil (VP) and Tetrodotoxin (TTX) for 2 seconds at 100 second interval	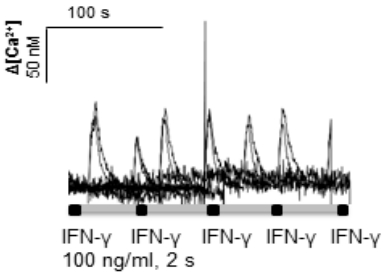	3 different preparations
D. 500 ng/mLIFN-γ in the presence of Verapamil (VP) and Tetrodotoxin (TTX) for 2 seconds at 100 second interval	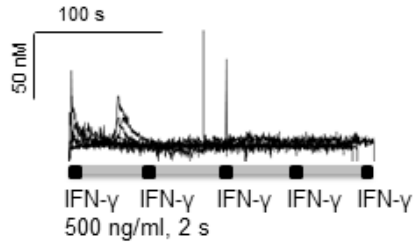	2 different preparations
E. 200 ng/mLIFN-γ in the absence of Verapamil (VP) and Tetrodotoxin (TTX) for 1.5-2 hours	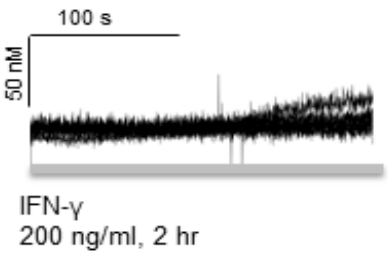	3 different preparations

4.1.4 IFN-γR1 expression is unchanged in the presence of hSOD1G93A gene in spinal motor neurons *in vitro*

To determine if hSOD1G93A gene influences IFN-γ's direct target, IFN-γR1, the distribution and basal expression of this subunit was examined in primary motor neurons *in vitro*. 13 day old primary co-cultures from both hSOD1G93A and non-transgenic mice were subjected to immunocytochemistry for IFN-γR1 along with the motor neuron marker, SMI32.

Upon visualizing under high magnification (63X oil immersion objective), IFN-γR1 was observed to be uniformly distributed across the motor neuron somas (Figure 10A) in both non-transgenic and hSOD1G93A motor neurons. Interestingly, signals were also observed in the nuclei of motor neurons from both the genotypes. Upon quantifying the immunofluorescence signals in the form of CTCF and comparing the values between non-transgenic (n = 60) and hSOD1G93A (n = 62), similar levels of IFN-γR1 (Figure 10B) were determined in the motor neurons. This was supported by quantitative PCR results that measured the relative mRNA levels for the receptor subunit in non-transgenic (n = 13) and hSOD1G93A (n = 11) (Figure 10C) motor neuron co-cultures.

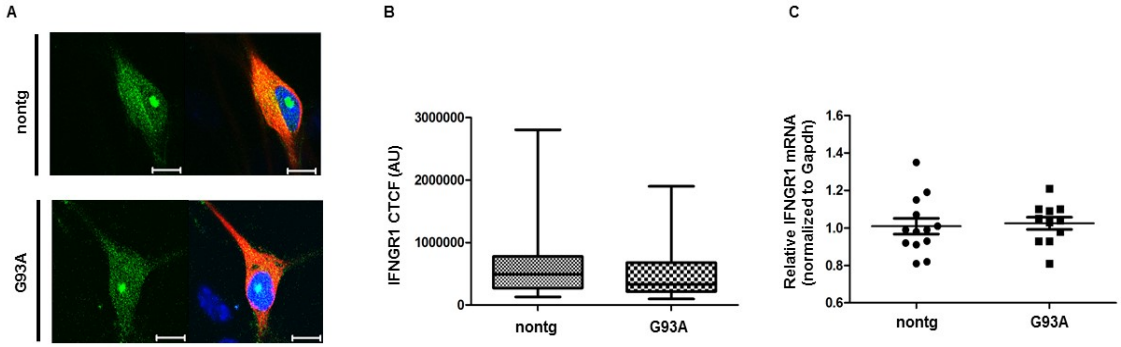

Figure 10. IFN-γR1 expression in embryonic motor neurons from primary co-culture. (A) IFN-γR1 observed in green channel is uniformly distributed across the somas of both hSOD1G93A (G93A) and non-transgenic (nontg) motor neurons. Scale bar = 10μm. (B) Protein expression measured as CTCF by immunofluorescence. CTCF of IFN-γR1 in G93A motor neurons (n = 62) was similar to that in nontg motor neurons (n = 60). (C) The relative expression of IFN-γR1 gene is normalised to GAPDH for nontg (n = 13) and G93A (n = 11) samples. The mRNA levels were similar in both the groups. Each column indicates mean ± SEM. Mann-Whitney test.

4.1.5 GluR1 levels similar in hSOD1G93A and non-transgenic motor neurons *in vitro*

Followed by determining IFN-©R1 levels, the expression of GluR1, the other principal target of the IFN-γ non-canonical pathway, in hSOD1G93A and non-transgenic motor neurons was analyzed *in vitro*. Immunostaining the primary motor neuron cultures for GluR1 along with SMI32 in both the genotypes revealed uniform distribution of the receptor subunit across the motor neuron somas (Figure 11A).

Protein levels were similar in hSOD1G93A (n = 45) and non-transgenic (n = 45) motor neurons as was observed from comparing the CTCF values (Figure 11B) in the motor neurons. The relative mRNA levels for GluR1 in non-transgenic (n = 13) and hSOD1G93A (n = 11) (Figure 11C) motor neuron co-cultures, also, supported the immunofluorescence observation.

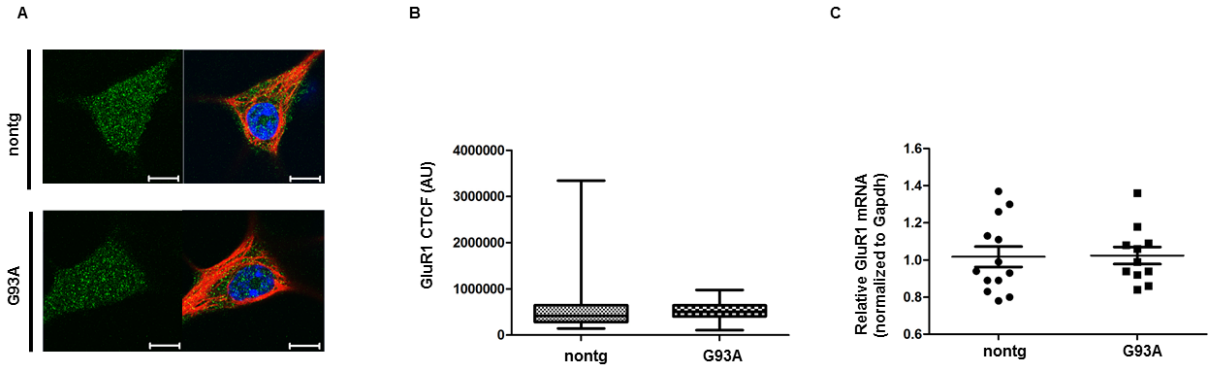

Figure 11. GluR1 expression in embryonic motor neurons studied in primary co-cultures. (A) Representative images of GluR1 that is uniformly distributed across the somas of both non-transgenic (nontg) and transgenic (G93A) motor neurons. Scale bar = 10 µm. (B) Protein expression measured as CTCF after immunofluorescence showed similar levels in G93A motor neurons (n = 45) and nontg motor neurons (n = 45). (C) The relative expression of GluR1 gene was normalised to GAPDH for nontg (n = 13) and G93A (n = 11) samples. The mRNA levels were similar in both the groups. Each column indicates mean ± SEM. Mann-Whitney test.

Taken together, the *in vitro* studies show that despite the presence of hSOD1G93A gene, direct application of IFN-γ neither significantly alters cytosolic calcium levels nor enhances kainate-mediated excitotoxicity. Moreover, expression of the principal receptor units, IFN-©R1and GluR1, was unchanged between the genotypes.

4.2 Ex vivo studies

4.2.1 Higher IFN-©R1 protein levels in motor neurons from cervical sections of both presymptomatic and symptomatic hSOD1G93A mice

Inflammation is mostly a late-stage event both in terms of lifespan and ALS disease. It is observed typically after disease onset. Thus, the pathway's principal targets were examined in adult mice *ex vivo*. Presymptomatic and symptomatic hSOD1G93A mice alongwith age-matched controls were used for the study. Cervical sections obtained from presymptomatic (Figure 12A) and symptomatic (Figure 12B) mice were immunostained and quantified for IFN-©R1 in the motor neurons. Two-way ANOVA following Bonferroni's post hoc correction for IFN-γR1 CTCF showed a significant effect of genotype ($F_{1,88} = 57.53$, p-value < 0.0001), unlike that of age ($F_{1,88} = 2.36$, p-value = 0.1285) or genotype x age interaction ($F_{1,88} = 1.51$, p-value = 0.2225) (Figure 12C) on IFN-γR1 expression.

4.2.2 Relative mRNA levels for IFN-©R1 similar in hSOD1G93A and non-transgenic mice

Relative mRNA levels of IFN-γR1 were, also, measured. For this purpose, whole spinal cords from symptomatic and presymptomatic mice were taken. The mRNA levels were normalized to the stable housekeeping gene hmbs. qPCR showed similar relative mRNA levels in both non-transgenic (9 weeks: n = 3, 17 weeks: n = 5) and hSOD1G93A (9 weeks: n = 6, 17 weeks: n = 8) mice (Figure 12D) in both the age groups.

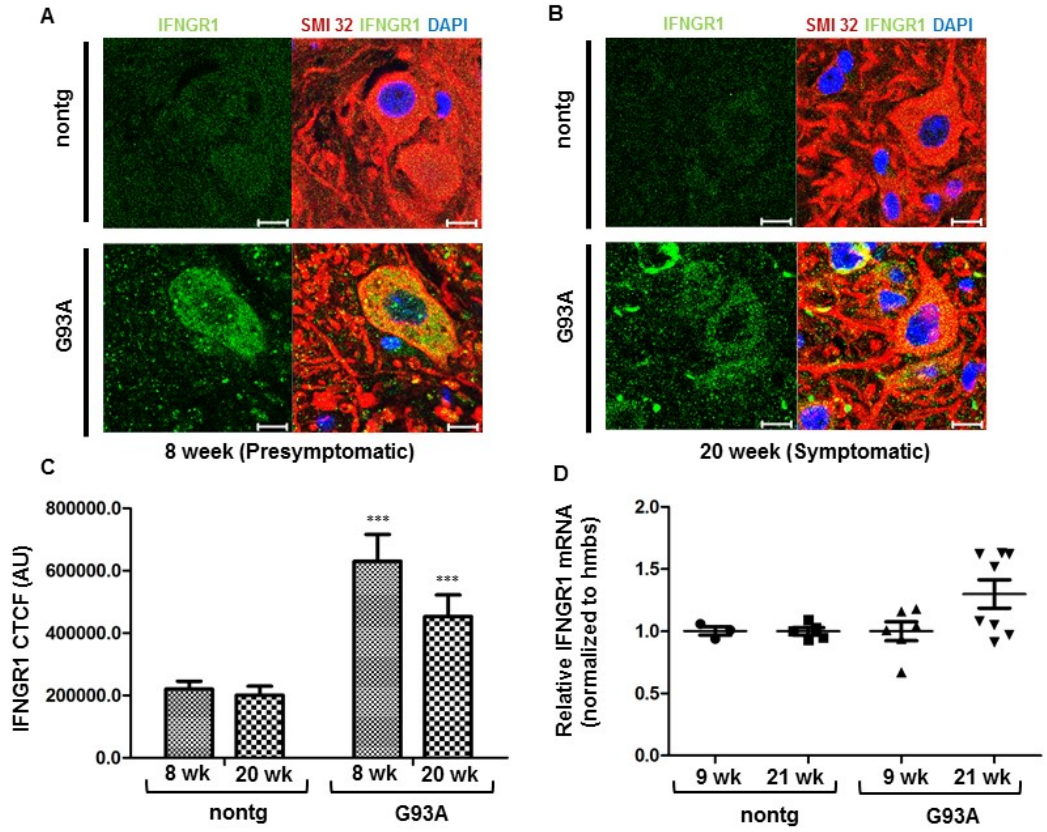

Figure 12. IFN-γR1 expression *ex vivo*. Images represent single-plane confocal scans of motor neurons in anterior horn of the cervical spinal cord section. Green channel shows IFN-γR1 protein expression in motor neurons of (A) presymptomatic and (B) symptomatic mice in both the genotypes. Scale bar = 10 µm. (C) IFN-γR1 protein expression was measured as CTCF (AU). Significantly increased IFN-γR1 CTCF was determined in motor neurons of both symptomatic (n = 45 from 3 mice) and presymptomatic (n = 45 from 3 mice) G93A mice when compared to age matched nontg controls (n = 45 from 3 mice for each age group). ***p ≤ 0.001. Two-way ANOVA with Bonferroni's correction. (D) Relative IFN-γR1 mRNA was similar in whole spinal cords of G93A (9 weeks: n=6, 21 weeks: n=8) mice when compared to age matched nontg controls (9 weeks: n=3, 21 weeks: n=5) irrespective of the age group. Mann-Whitney test between every two groups. Data presented as scatter plots in one graph as mean ± SEM.

4.2.3 Elevated GluR1 in cervical sections of symptomatic hSOD1G93A mice motor neurons

Expression of the pathway's other principal primary target, GluR1, was studied. Cervical sections sliced from spinal cords of presymptomatic (Figure 13A) and symptomatic (Figure 13B) mice were immunostained and quantified for GluR1 in the motor neurons. On comparing CTCF values using two-way ANOVA, a significant effect of genotype ($F_{1,88}$ = 20.36, p-value = 0.002) and genotype x age interaction ($F_{1,88}$ = 13.96, p-value = 0.0104), unlike that of age ($F_{1,88}$ = 1.11, p-value = 0.2874) was observed for GluR1 expression (Figure 13C).

4.2.4 Similar relative mRNA levels of GluR1 in hSOD1G93A and non-transgenic mice

Whole spinal cords from both hSOD1G93A and non-transgenic mice for both age groups were collected for relative mRNA measurement of GluR1. The housekeeping gene hmbs expression was employed for normalization. Similar levels of mRNA were observed in both the genotypes irrespective of age group: non-transgenic (9 weeks: n = 3, 17 weeks: n = 5) and hSOD1G93A mice (9 weeks: n = 6, 17 weeks: n = 8) (Figure 13D)

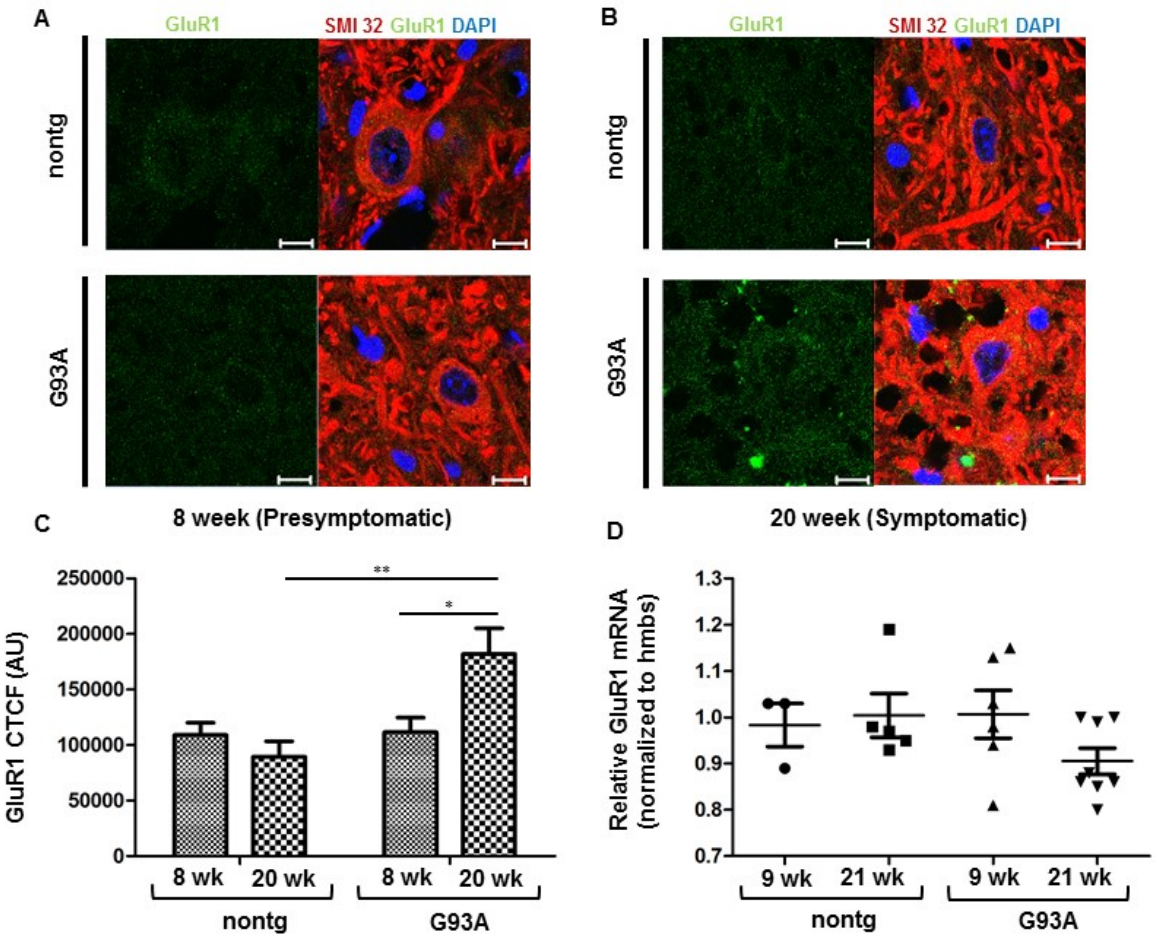

Figure 13. GluR1 expression *ex vivo*. Images represent single-plane confocal scans of motor neurons in anterior horn of the cervical spinal cord section. Green channel shows GluR1 protein expression in motor neurons of (A) presymptomatic and (B) symptomatic mice in both the genotypes. Scale bar = 10 µm. (C) GluR1 protein expression was measured as CTCF (AU). Significantly increased GluR1 CTCF was determined in motor neurons of symptomatic G93A mice (n = 45 from 3 mice) as against presymptomatic (n = 45 from 3 mice) group and age-matched nontg control (n = 45 from 3 mice). **p = 0.002, *p = 0.0104. Two-way ANOVA with Bonferroni's correction. (D) Relative GluR1 mRNA is similar in whole spinal cords of G93A (9 weeks: n=6, 21 weeks: n=8) mice when compared to age matched nontg controls (9 weeks: n=3, 21 weeks: n=5) irrespective of the age group. Mann-Whitney test between every two groups. Data presented as scatter plots in one graph as mean ± SEM.

4.2.5 Similar JAK1 levels in adult hSOD1G93A and non-transgenic mice motor neurons.

With primary participants of the IFN-γ mediated neuron-specific pathway detected at elevated levels, especially in the symptomatic hSOD1G93A mice, the next step was to investigate the expression of the pathway's key downstream players, namely JAK1, phosphorylated STAT1, and Protein Kinase A (PKA). JAK1 protein expression was examined in spinal motor neurons of presymptomatic as well as symptomatic hSOD1G93A mice and their age-matched non-transgenic controls. Cervical sections were stained for SMI32, the selective motor neuron marker, and the target protein JAK1. The signaling protein was distributed uniformly across the cell somas (Figure 14A, 14B). Comparing the CTCF values from non-transgenic and hSOD1G93A by two-way ANOVA revealed no significant effects of genotype ($F_{1,88} = 3$, p-value = 0.0876), age ($F_{1,88} = 3.39$, p-value = 0.07) and genotype x age interaction ($F_{1,88} = 1.61$, p-value = 0.2089) (Figure 14C). Relative mRNA levels of JAK1 from whole spinal cords of hSOD1G93A (9 weeks: n=6, 17 weeks: n=8) and non-transgenic (9 weeks: n=3, 17 weeks: n=5) were, also, similar (Figure 14D).

4.2.6 Unchanged STAT1 levels in motor neurons from hSOD1G93A and non-transgenic adult mice

Phosphorylated STAT1 is a measure of active JAK1/STAT1 signaling. Examining its expression could, thus, give an estimate of the degree of activation in the spinal motor neurons from hSOD1G93A and non-transgenic mice. Sections from cervical regions were stained for SMI32 and phosphorylated STAT1 for mice from both the genotypes. The CTCF values were unchanged as demonstrated by insignificant effects of age ($F_{1,88} = 1.39$, p-value = 0.2438), genotype ($F_{1,88} = 3.34$, p-value = 0.0732), and genotype x age interaction ($F_{1,88} = 0.35$, p-value = 0.5548) (Figure 15C). Measuring relative levels of STAT1 mRNA yielded similar expression in whole spinal cords of both presymptomatic and symptomatic hSOD1G93A mice (9 weeks: n=6, 17 weeks: n=8) and their age-matched controls (9 weeks: n=3, 17 weeks: n=5) (Figure 15).

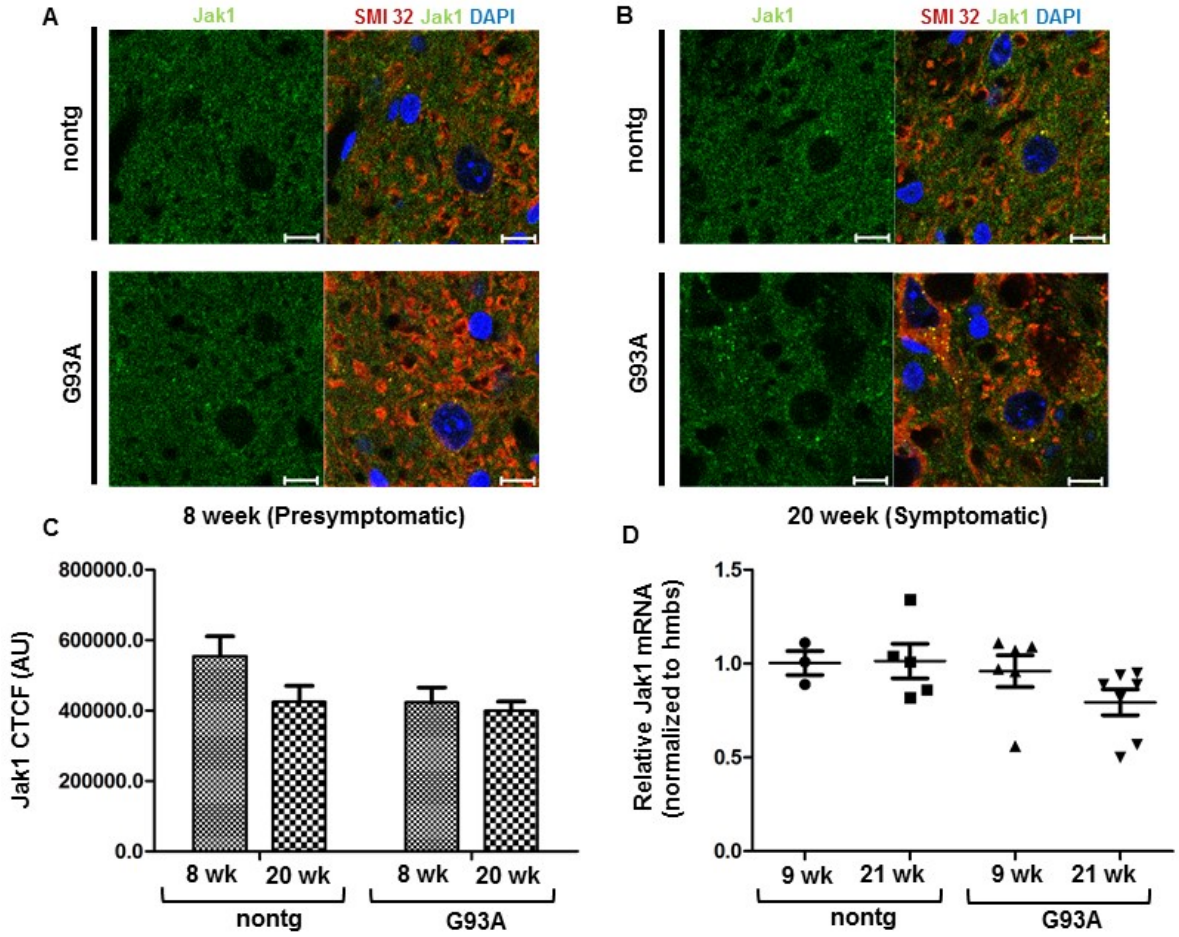

Figure 14. ***Ex vivo*** **Jak1 expression.** Green channel shows Jak1 expression in cervical sections of both (A) presymptomatic and (B) symptomatic mice for both the genotypes. Scale bar = 10 μm. C) Jak1's CTCF was similar in both nontg (n = 45 from 3 mice for each age group) and G93A mice (n = 45 from 3 mice for each age group) Two-way ANOVA with Bonferroni's correction (D) Jak1 mRNA is similar in spinal cords of G93A mice (9 weeks: n=6, 17 weeks: n=8) when compared to age matched nontg controls (9 weeks: n=3, 17 weeks: n=5) irrespective of the age group. Mann-Whitney test between every two groups. Data presented as scatter plots in one graph as mean ± SEM.

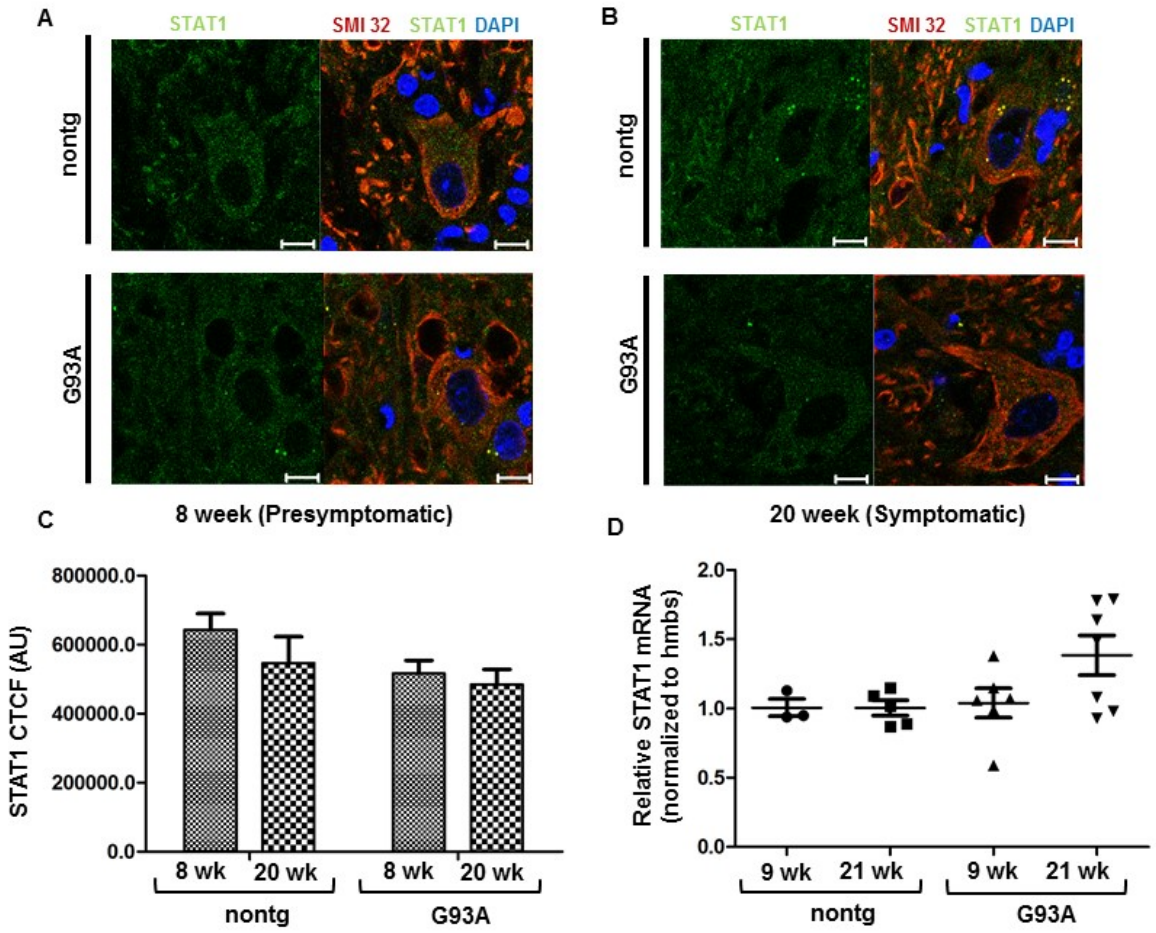

Figure 15. *Ex vivo* Stat1 expression. Green channel reflects Stat1 expression in cervical sections of both (A) presymptomatic and (B) symptomatic mice for nontg and G93A genotypes. Scale bar = 10 μm. C) Stat1 CTCF was similar in both nontg (n = 45 from 3 mice for each age group) and G93A mice (n = 45 from 3 mice for each age group) Two-way ANOVA with Bonferroni's correction (D) Stat1 mRNA is similar in whole spinal cords of G93A mice (9 weeks: n=6, 17 weeks: n=8) when compared to age matched nontg controls (9 weeks: n=3, 17 weeks: n=5) in both symptomatic and presymptomatic groups. Mann-Whitney test between every two groups. Data presented as scatter plots in one graph as mean ± SEM.

4.2.7 Lowered expression of one of the catalytic subunits of Protein Kinase A in symptomatic hSOD1G93A mice

JAK1/STAT1 signaling increases cellular cAMP that activates Protein Kinase A, which in turn phosphorylates GluR1 at position serine 845. With levels of JAK1 and activated STAT1 similar between non-transgenic and hSOD1G93A motor neurons, the transcript expression of the catalytic subunits of PKA – PKAa and PKAb – were determined. In whole spinal cords from symptomatic hSOD1G93A mice, relative mRNA levels of PKAa were significantly lower as against those in age-matched control and presymptomatic mice. PKAb levels remained unchanged irrespective of the age group or genotype (Figure 16).

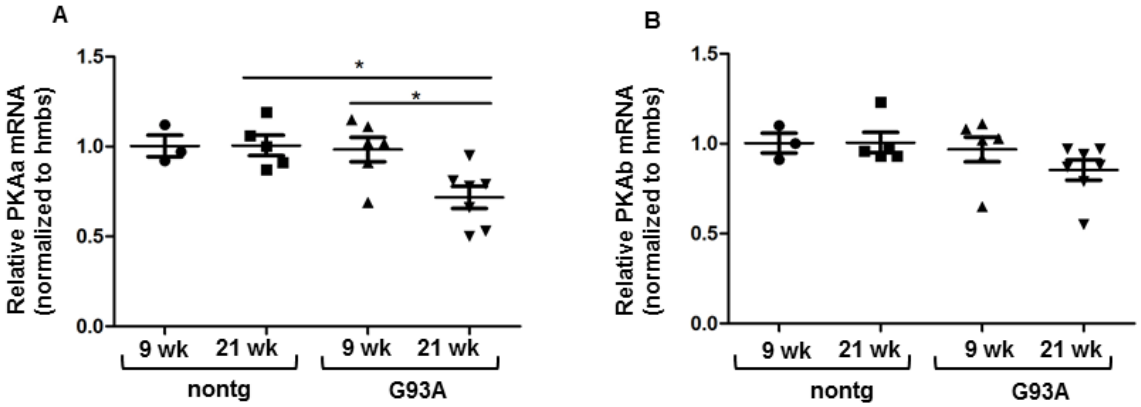

Figure 16. Protein Kinase A expression *ex vivo*. (A) PKAa mRNA is lower in whole spinal cords of hSOD1G93A symptomatic mice (17 weeks: n = 8) when compared to age-matched nontg controls (9 weeks: n = 3, 17 weeks: n = 5) and presymptomatic hSOD1G93A mice (9 weeks: n = 6). However, (B) PKAb mRNA levels remained unchanged irrespective of symptom group in both nontg (9 weeks: n = 3, 17 weeks: n = 5) and hSOD1G93A (9 weeks: n = 6, 17 weeks: n = 8) mice. Mann-Whitney test between every two groups. Data presented as scatter plots in one graph as mean ± SEM. *$p < 0.05$.

5. DISCUSSION

Calcium dysregulation and neuroinflammation have been well implicated in ALS as key pathogenic factors. This study shows that the ligand-binding subunit of the pro-inflammatory cytokine, IFN-©, called IFN-©R1 is upregulated in spinal motor neurons of adult hSOD1G93A mice in both presymptomatic and symptomatic stages of the disease. Moreover, GluR1, a subunit of AMPARs, that is involved in calcium dysregulation in ALS is enhanced in the motor neurons of symptomatic hSOD1G93A mice. These two receptor subunits, IFN-©R1 and GluR1, are primary participants of a non-canonical neuron-specific IFN-© pathway that is known to function via JAK1/STAT1 signaling upon IFN-© stimulation and inducing calcium influx (Mizuno *et al.*, 2008). Upon examining the expression of the pathway's downstream participants, this study shows similar levels of JAK1/STAT1 in motor neurons of both hSOD1G93A and non-transgenic mice *ex vivo*, unlike that of PKA wherein the transcript level of one of its catalytic subunits is lower in the spinal cords of symptomatic hSOD1G93A mice. Moreover, the ALS mutation carrying gene, hSOD1G93A, alone does not influence the expression of IFN-©R1 and GluR1, as seen in the expression studies of the subunits *in vitro*, which is representative of embryonic/early postnatal stage. Additionally, studying the functional effects of IFN-© *in vitro* reveals that the cytokine is weakly neurotoxic as it induces neuronal damage in spinal motor neurons observed as dendritic beads, but does not significantly alter cytosolic calcium levels or motor neuron survival *in vitro*. These functional effects would most likely be enhanced in the adult hSOD1G93A wherein higher levels of IFN-©R1 are present in the motor neurons. Thus, principally, this study presents IFN-©R1 as a potential target that could not only directly link neuroinflammation and neurodegeneration in ALS, but could also be modulated to regulate ALS progression.

Despite several years of extensive research, ALS pathogenesis is still complex and not very well understood. Motor neuron death from excessive calcium influx due to over-stimulation of mostly AMPA receptors has been well documented, especially in the context of ALS. High calcium entry is often regarded as the maleficent force behind AMPAR mediated excitotoxic motor neuron death in ALS (Grosskreutz *et al.*, 2010; Patai *et al.*, 2016). Ironically, despite being susceptible to excitotoxicity, motor neurons did not evolve to house sufficient levels of calcium-binding proteins and exhibit lower density of mitochondria per cell volume to buffer the cytosolic calcium (Grosskreutz *et al.*, 2007; Tadic *et al.*, 2014). This paradox can be

explained by the physiological need of the motor neurons to activate rapidly and efficiently via calcium cycling for muscle contraction and expansion. Presence of good calcium buffering system would mean lack of readily available free calcium for signaling and other associated molecular processes.

Neurodegeneration in ALS is mostly from activation of inflammatory pathways involving stimulated microglia and infiltrating lymphocytes. There are several studies on cellular players and molecular mechanisms of neuroinflammation in ALS (Liu & Wang, 2017). However, there is no record till date that focuses on a pathway that could directly link motor neuron degeneration and neuroinflammation along the axis of calcium dysregulation, a key common denominator in ALS pathogenesis (Patai *et al.*, 2016). In one previous study, cortical neuron dysfunction via calcium influx was demonstrated upon IFN-© stimulation *in vitro* in healthy mice. Following up on this study, the present work focuses on studying the involved pathway in spinal motor neurons in both the hSOD1G93A ALS mouse model and healthy non-transgenic mice. Including the latter kind not only helped serve the purpose of having a natural non-transgenic control, but also gain insights in healthy cases. Moreover, the pathway was examined in motor neurons both *in vitro*, which represents the embryonic stage, as well as *ex vivo* in adult mice.

5.1 Dendritic beads in hSOD1G93A and non-transgenic motor-neuron co-cultures

Neuritic beading is an early hallmark of neuronal toxicity that has been reported in several pathological conditions like Alzheimer's disease, Amyotrophic Lateral Sclerosis, CNS trauma, and other related conditions (Delisle & Carpenter, 1984; Hori & Carpenter, 1994; Takahashi *et al.*, 1997; Dickson *et al.*, 1999; Mattila *et al.*, 2000; Swann *et al.*, 2000; Goel *et al.*, 2003; Saito *et al.*, 2003). Cellular events that trigger the focal bead-like swelling include stimuli from glutamate, oxidative stress, hypoxia, and hypotonic conditions. The functional role of these beads in pathological conditions is still unclear. Excitotoxic stimulus triggers influx of water along with sodium and chloride ions in neurons to induce bead formation by mechanisms that are unknown till date. Subsequent calcium entry maintains the morphological changes in the damaged dendrites (Hasbani *et al.*, 1998). Interestingly, IFN-γ has, also, been shown to induce dendritic beads *in vitro* in primary mouse cortical neuron cultures (Mizuno *et al.*, 2008).

In this study, to determine if this neurotoxic effect of IFN-© is recapitulated in spinal motor neurons, primary motor neuron-astrocyte co-cultures from both hSOD1G93A and non-transgenic mice were incubated with IFN-γ for 12 hr. Dendritic beads were observed in both the genotypes when compared to neurons from untreated co-cultures. This could be due to the functioning of the IFN-©R1:GluR1 pathway as demonstrated in the previous cortical neuron study (Mizuno *et al.*, 2008). Another explanation could be low numbers of microglia that get activated by IFN-γ and induce neuritic beading (Takeuchi *et al.*, 2005). However, if it is glial-cell mediated, the beading process most likely would take more than 12 hours considering the involvement of an intermediate participant. Nevertheless, this observation indicates the neurotoxic effect of IFN-γ, irrespective of the presence of hSOD1G93A gene.

5.2 AMPAR-mediated excitotoxicity unaffected by IFN-γ

Dendritic beading implies that IFN-γ works on the primary motor neuron co-cultures and induces damage. To further explore its neurotoxic role, the cell cultures from both genotypes were treated with IFN-γ and kainate (a potent AMPAR agonist) in combination or alone for 12 & 24 hr.

Sole application of IFN-γ to our primary motor neuron-enriched co-cultures did not kill the motor neurons. This observation that IFN-γ is independently not lethal to the motor neurons supports similar previous studies of the cytokine on neurons (Mizuno *et al.*, 2008; O'Donnell *et al.*, 2015). Interestingly, in a different study, hSOD1G93A astrocytes releasing IFN-γ was shown to induce neuronal death to similar degrees in both wild-type hSOD1 and hSOD1G93A motor neurons in a LIGHT-dependent manner (Aebischer *et al.*, 2010). However, it would be important to note that this apparent lethal effect was observed only at disease onset and symptomatic stage of the ALS mouse model implying significant neurotoxic effects of IFN-γ via astrocytes mostly during ALS progression.

Additional observation in our cell survival study was the AMPAR-mediated excitotoxicity that was unaffected by IFN-γ. This was interesting as it contrasted with similar study on cortical neurons (Mizuno *et al.*, 2008). There are a few possibilities that can explain this detection apart from the fact that a different AMPAR agonist was used in the previous study as against the current one.

Firstly, motor neurons have a high concentration of AMPARs and are highly vulnerable to kainate. This agonist incessantly binds to AMPARs and mediates excitotoxic death via fast kinetic reaction. On the other hand, IFN-γ induced neurotoxicity via IFN-©R1:GluR1 receptor complex formation requires activation of a pathway involving a cascade of steps that could be more time-consuming (Figure 17). Secondly, IFN-γ is not lethal to motor neurons *in vitro* and induces only weak neurotoxicity that demonstrated as dendritic beads. Taken together, this suggests that combining both kainate and IFN-γ could result in a neurotoxic response wherein the weak effect of IFN-γ is most likely masked by the strong excitotoxic kainate response. This is corroborated in the 24 hr study wherein percentage of surviving motor neurons further decreases to extremely low numbers with kainate as against hardly any changes in motor neuron survival that underwent IFN-γ treatment alone. Thirdly, Major Histocompatibility Complex-1 (MHC-1) on motor neurons can, also, influence its susceptibility to neurotoxicity. This happens in two ways: IFN-γ upregulates MHC-1 in motorneuron-astrocyte co-cultures (Nardo *et al.*, 2016) that can lead to enhanced AMPAR trafficking (Fourgeaud *et al.*, 2010), thus, culminating in higher calcium influx upon AMPARs stimulation alone. On the other hand, hSOD1G93A astrocytes can lower MHC-1 expression in motor neurons and make them more vulnerable to neurotoxicity (Song *et al.*, 2016). Among the two aforementioned ways, the former could most likely be a reason behind our cell survival study's observation as the latter was demonstrated only in symptomatic hSOD1G93A mice. Finally, IFN-γ is known to activate protective non-canonical signaling in primary neurons via Erk1/2 involving pathway (O'Donnell *et al.*, 2015) and this could be considered as a standalone explanation behind unaffected AMPAR-mediated excitotoxicity. However, bringing the observation of dendritic beads into the picture, it can be stated that the protective non-canonical signaling is most likely not activated in the motor neurons from our cell survival study.

As for the apparent contrasting observations of the survival study with the dendritic beading observation, it would be critical to note that formation of the beads is a much more rapid process as compared to calcium-mediated excitotoxic injury (Hasbani *et al.*, 1998). Hence, it could be that the IFN-γ induces neurotoxicity, but enhancing AMPAR mediated excitotoxicity might be a slower and weaker process in hSOD1G93A motor neurons.

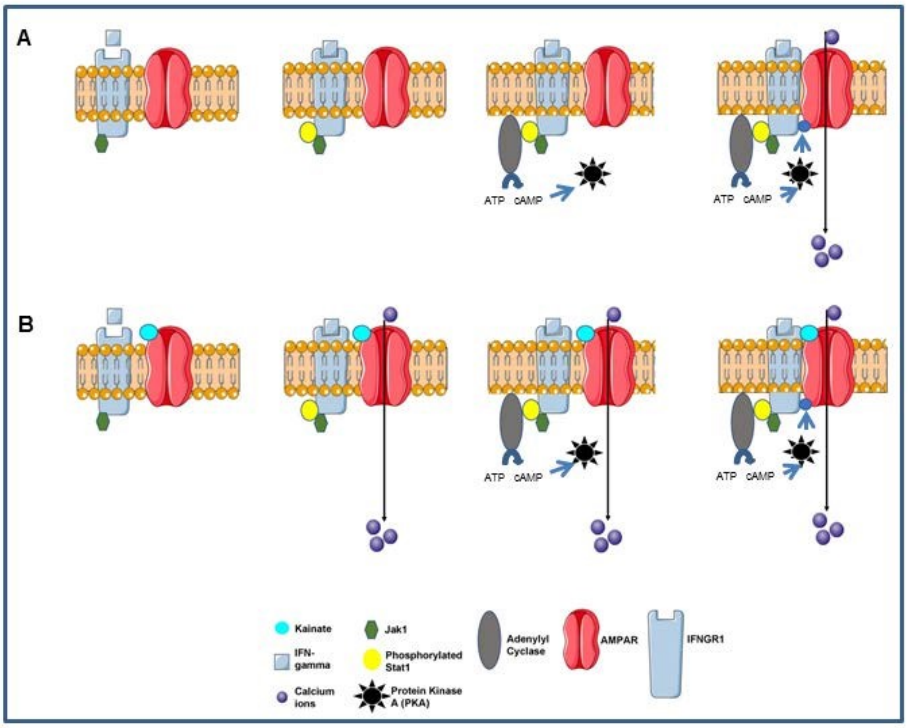

Figure 17. Hypothetical model explaining kainate-mediated excitotoxicity unaffected by IFN-γ. (A) IFN-γ binds to IFN-©R1 leading to downstream activation of JAK1 and recruitment of STAT1 following phosphorylation. Phosphorylated STAT1 activates adenylyl cyclase, which in turn increases cAMP levels resulting in activation of PKA and subsequent phosphorylation of GluR1 subunit of AMPAR. This induces formation of a neuron-specific calcium permeable receptor complex between AMPAR and IFN-©R1. (B) When both kainate and IFN-γ are present, fast-kinetic reaction occurs wherein kainate incessantly opens the AMPAR to allow calcium entry. In contrast, IFN-γ follows sequential steps to mediate formation of calcium-permeable complex with already active AMPARs.

5.3 Weak single cell calcium responses from neurons of hSOD1G93A and non-transgenic motor-neuron co-cultures upon direct IFN-γ treatment

Upon IFN-γ stimulation, neuronal damage due to excessive calcium influx in cortical neurons has been observed in previous study (Mizuno *et al.*, 2008). Moreover, AMPAR stimulation by potent agonists like kainate triggers neuronal death by inducing intracellular calcium influx, which is enhanced in hSOD1G93A motor neurons (Grosskreutz *et al.*, 2010). Apart from studying the effect of IFN-γ on neuronal survival, this study examined the effect of the cytokine on cytosolic calcium levels.

For our motor neuron co-culture system, several protocols were tested to elicit a strong calcium signal in the single cell measurements: low doses (100 ng/ml, 200 ng/ml) and high dose (500 ng/mLIFN-γ) direct short and long-term application both in the presence and absence of other channel blockers; pre-incubation with IFN-γ followed by kainate stimulation in the presence and absence of other channel blockers. In all the tested experimental conditions, the cytosolic calcium responses were weak and inconsistent, thus, implying that IFN-γ is most likely directly triggering calcium influx, but is not potent enough to elicit a large signal. The weak responses can be due to the possible presence of this receptor complex majorly in the extrasynaptic region as compared to the synapses as suggested in a previous study (Mizuno *et al.*, 2008). This can be confirmed in future studies with electrophysiological recordings, a theme that is beyond the scope of this study. Moreover, the occasional spontaneous calcium transients observed as asynchronous signals in the absence of the channel blockers (Table 17.C) demonstrate that the signals were from live neurons that were unperturbed by mechanical application of the cytokine (Grosskreutz *et al.*, 2007). To compare the strength of the calcium signals from IFN-γ and confirm that the cultures were alive, independent measurements after sole kainate application were, also, done in parallel (Figure 18).

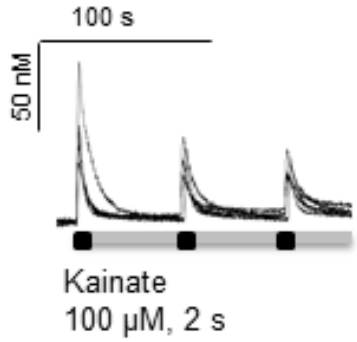

Figure 18. Representative cytosolic calcium measurements from kainate stimulation. AMPARs of spinal motor neurons were stimulated with 100 µM kainate for 2 seconds at every 100 second interval in the presence of verapamil and TTX.

5.4 IFN-γR1 expression in hSOD1G93A motor neurons

Apart from intracellular calcium, IFN-γ also regulates several immune responses. In hSOD1G93A mice, cytokine profiling showed high levels of IFN-γ throughout the ALS disease course starting from onset (Michaelson *et al.*, 2017). However, expression of its receptor's ligand binding unit, IFN-γR1, has not been investigated till date in ALS. Classical IFN-γ pathway involves participation of ligand binding IFN-γR1and signal transducing IFN-γR2 subunits of the IFN-γ receptor. For this piece of work, IFN-γR1 is our target of interest.

We examined the distribution and expression of the receptor subunit initially in primary motor neurons that represent embryonic stage in both hSOD1G93A and non-transgenic motor

neuron-astrocyte co-culture systems. Both relative mRNA and protein levels were measured by qPCR and immunofluorescence methods respectively.

Our experiments revealed similar levels of IFN-γR1 expression at both mRNA and protein levels, irrespective of the genotypes *in vitro*. It is known that IFN-γR1 is constitutively expressed on all cell types at moderate level (Bach *et al.*, 1997). Thus, our observation in mice primary motor neurons suggests that hSOD1G93A presence does not alter expression or distribution of the receptor subunit atleast in the embryonic stage. The receptor subunit was uniformly distributed across the cell somas, apart from a concentrated signal in the nucleus. This could most likely be from certain fraction of IFN-γR1 that translocated to the nucleus to regulate gene expression (Ahmed & Johnson, 2006).

Considering that the immune cells of the CNS acquire inflammatory phenotype with age and/or disease progression(Fenn *et al.*, 2015), expression of IFN-γR1 was, also, examined in the motor neurons of adult hSOD1G93A mice. Since the pattern of disease spread in this mouse model is from lumbar to cervical region (Beers *et al.*, 2011), the spinal cord sections for IFN-γR1 protein study were taken from the cervical regions of hSOD1G93A mice and their age-matched controls. For relative mRNA measurements, whole spinal cords were employed. Considering that IFN-γ levels are higher in motor neurons from spinal cords of diseased hSOD1G93A mice, IFN-γR1 also should be ideally upregulated. True to the hypothesis, IFN-γR1 protein levels were higher in motor neurons of symptomatic hSOD1G93A mice as against their age-matched controls. Surprisingly, the receptor unit was upregulated in motor neurons of presymptomatic hSOD1G93A mice, too. It is to be noted here that IFN-γR1 expression can be enhanced by proinflammatory cytokines like TNF-α and IL-1β, which are elevated at early stages in hSOD1G93A mice (Michaelson *et al.*, 2017). Additionally, post-translational modifications could potentially be elevated in hSOD1G93A mice that lead to receptor stability (Londino *et al.*, 2017). These studies, also, explain the reason for lack of enhanced IFN-γR1 expression in embryonic hSOD1G93A motor neurons.

In contrast to the protein expression studies, relative mRNA measurements from whole spinal cords reveal no change in expression. Apart from reasons stated for elevated IFN-γR1expression in motor neurons, an additional explanation for the mRNA results could be the fact that the IFN-γR1 signal in the qPCR comes from a plethora of cells with motor neurons

constituting only a fraction of the cell population. mRNA measurements exclusively from cervical regions were not attempted owing to very low amounts of generated cDNA sample. Collectively, the IFN-γR1expression results suggest that mere hSOD1G93A gene presence does not influence the receptor subunit's expression and that this is most likely regulated by several physiological factors in the adult mice.

Presence of high levels of IFN-γR1 imply priming of hSOD1G93A motor neurons to immune responses and being susceptible to IFN-γ associated signaling even before disease onset. To our knowledge, this is the first study on IFN-γR1 expression in spinal motor neurons of any ALS mouse model.

5.5 GluR1 expression in motor neurons of hSOD1G93A mice

GluR1 is one of the key AMPAR subunits that is present in spinal motor neurons and contributes to their excitotoxic death. For our study, similar to IFN-γR1expression analysis, we initiated examining the expression of GluR1 with primary motor neuron co-cultures that are representative of embryonic/early postnatal period. Both mRNA and protein expression analyses revealed unchanged GluR1 expression despite the presence of hSOD1G93A gene. This supports the fact that GluR1 is developmentally regulated in spinal motor neurons (Jakowec, Yen, *et al.*, 1995).

Expression study in motor neurons from adult spinal cords revealed barely detectable levels of GluR1 in presymptomatic hSOD1G93A mice and their age-matched control. This observation is in sync with a previous study that showed that levels of GluR1 decrease with age in healthy rat spinal cord in a fashion such that by adulthood, the motor neurons express very low to no levels of the subunit transcript (Jakowec, Fox, *et al.*, 1995).

However, in the symptomatic hSOD1G93A motor neurons, elevated levels of GluR1 were observed as against barely detectable levels in the motor neurons from age-matched control. In an earlier study, total GluR1 levels in spinal motor neurons of presymptomatic hSOD1G93A mice were observed to be higher at 17 weeks of age when compared to those from hSOD1 wildtype controls (Zhao *et al.*, 2008). But, this was not observed in hSOD1G93A mice that were younger than 17 weeks. This implies that with age, GluR1 levels most likely increase in motor neurons of hSOD1G93A mice, thus, supporting our study.

Moreover, high levels of MHC-1 in symptomatic mice can positively regulate expression of GluR1 on membrane surface (Fourgeaud *et al.*, 2010). Another explanation behind elevated GluR1 in motor neurons of symptomatic hSOD1G93A mice is the subunit's upregulation by cytokines like TNF-α that are increased in the spinal cords of ALS mice (Stellwagen *et al.*, 2005). Elevated GluR1 levels, also, suggest changes in dendritic complexity and in the diseased case, this might contribute to abnormal motor movements (Inglis *et al.*, 2002; Prithviraj *et al.*, 2007), a feature observed in ALS.

5.6 Unchanged JAK1 levels in adult hSOD1G93A mice motor neurons *ex vivo*

Primary targets of the neuron-specific IFN-γ pathway were overexpressed in adult hSOD1G93A mice motor neurons, especially in the symptomatic stage. To determine if the pathway is overall upregulated, measuring expression of key downstream targets is, also, essential. The first downstream target involved in this non-canonical signaling is JAK1. Measuring relative mRNA and protein levels demonstrated similar JAK1 levels between hSOD1G93A and non-transgenic mice irrespective of the disease stage. Studies on differential expression of inflammation related genes in hSOD1G93A mice revealed JAK3 as the only member from the Janus Kinase family that was upregulated in both presymptomatic and symptomatic ALS mice (Yoshihara *et al.*, 2001). This implies that JAK1 expression is unchanged throughout the disease course, which supports our observation. Moreover, cellular JAK1 is associated with other proteins, also, apart from IFN-γR1. Thus, increased IFN-γR1 need not necessarily correlate with high levels of JAK1. The expression of this downstream target was not examined in primary motor neuron culture considering similar expression levels of the primary targets, IFN-γR1 & GluR1.

5.7 Similar levels of activated STAT1 in adult hSOD1G93A and non-transgenic mice motor neurons *ex vivo*

Regarding the STAT members, while some STATs like STAT2, STAT4, and STAT6 have specific activation patterns, others like STAT1 and STAT3 can be activated by several cytokines (Pestka *et al.*, 1997). Phosphorylated STAT1 (pSTAT1) is the activated form of STAT1, whose expression was examined in motor neurons *ex vivo* in the present study.

pSTAT1 is known to be upregulated in astrocytes of presymptomatic hSOD1G93A mice. Interestingly, unlike astrocytes, motor neurons from hSOD1G93A mice in our study showed similar pSTAT1 levels when compared to age-matched controls, irrespective of the disease stage. This was, also, supported by mRNA results. Similar STAT1 levels along with unchanged JAK1 levels indicate that although the surrounding milieu of the motor neurons have upregulated JAK1/STAT1 signaling induced by IFN-γ in hSOD1G93A, the signaling is most likely not enhanced in the neurons themselves. This could be an attempt to counter balance inflammatory reactions, notwithstanding the presence of higher levels of IFN-γR1.

These results, also, throw light on the complexity of receptor signaling in neurodegenerative conditions like ALS wherein some of the players are upregulated while many others are not. As was for JAK1, the expression study of STAT1 also was not attempted in motor neuron co-cultures.

5.8 Decreased expression of one of the two catalytic subunits of PKA in symptomatic hSOD1G93A mice *ex vivo*

Protein Kinase A (PKA) is the best described kinase member of the protein kinase superfamily that is principally involved in modifying proteins by phosphorylating them. Its activity is dependent on intracellular cAMP whose levels are regulated by the enzyme adenylyl cyclase. Functional mouse PKA has 2 catalytic isoforms in action: PKAa and PKAb. As a form of preliminary investigation, the transcript levels of these catalytic isoforms were analyzed in this study. Although relative mRNA levels of PKAb in hSOD1G93A mice were similar to non-transgenic age-matched controls, lower PKAa mRNA levels were observed in symptomatic hSOD1G93A mice. This implies that there could be a downregulation in PKA activity post disease onset. Expression study of protein kinases and phosphatases in spinal cords of hSOD1G93A mice revealed unchanged PKA expression (Hu *et al.*, 2003) as against wild-type hSOD1 controls. The digression in our expression study could be due to use of non-transgenic animals as against wild-type hSOD1 as the control system. Additionally, decreased PKA signaling has been observed in neurodegenerative disorders (Dagda & Das Banerjee, 2015) that supports our preliminary observation of PKA levels. Combining our results on downstream targets with previous studies presents the complexity of this non-canonical IFN-γ signaling in adult hSOD1G93A mice and the need for a full-fledged independent study to examine the cascading events in further detail in adult mice.

5.9 Strengths and limitations of the study

The study's experimental framework utilized both the well-established motor neuron-enriched primary cell culture system as well as adult spinal cord cervical sections from hSOD1G93A mice and the non-transgenic controls. While the former system is representative of embryonic stage, the *ex vivo* studies gave insights into the pathway in motor neurons from adult mice spinal cords. The primary motor neuron co-culture system presents several advantages for investigating neurodegeneration in ALS. First, the primary cell cultures reflect disease features more accurately than immortalized cell lines. Second, co-cultivation with astrocyte glia bears semblance to the actual physiological state of the neurons in the spinal cord wherein the neurons are in a glial cell environment. Most importantly, the parallel cultivation of transgenic (ALS) and non-transgenic (control) cells can define disease-specific molecular characteristics. However, primary cell culture preparation doesn't lend itself to sample-intensive techniques like Western Blotting. Moreover, the inability to physically extract mature motor neurons from glial feeder layers also renders mixed signals in qPCR. The observation of dendritic beads could have been supported by a co-localization study of the receptor complex, but considering the available resources including time and the fact that the cytokine exerted minimal functional changes, this additional experiment would add more value if done in future studies involving *ex vivo* specimens rather than *in vitro*. It is, also, critical to note that although disease-associated proteins or pathways are examined in the hSOD1G93A mouse system, such animal models never fully recapitulate the disease as it is observed in humans. For instance, the transgene gross overexpression used to generate the hSOD1G93A model results in toxic offshoots that significantly accelerate the disease course to the degree that measuring a clinically relevant outcome becomes very difficult (Zwiegers & Shaw, 2015).

The *ex vivo* studies might bear more similarity to the disease pathology in patients than *in vitro* cell culture studies. Whole spinal cords from adult mice were employed for the expression studies. Motor neurons were imaged from spinal cord sections and protein expression was analyzed using standard expression analysis methods like ImageJ. mRNA expression analyses for the targets of interest were, also, carried out. This resulted in a clearer picture of the expression of the key upstream and downstream participants of the non-canonical neuron-specific IFN-γ pathway in the disease model, unlike in the case of pure gene expression approach *in vitro* wherein the gene expression itself may or may not reflect the actual protein expression.

Motor neurons were identified by SMI32 staining and the targets of interest found only in these neurons were evaluated. Western blots employing whole spinal cords implied that the target mRNA values would be from the all the different cell types and, hence, were not carried out. Due to the lack of a cell isolation arrangement that would help isolate pure motor neurons from the anterior horn spinal cord grey matter, immunofluorescence based approach was used for protein expression. The imaging for *ex vivo* protein expression has not been performed on a perfect three-dimensional cut-out of target cells owing to absence of an ultra-high resolution imaging system and software that could demarcate cells along their respective membranes either manually or automatically. The analyzed z-stacks contain irregularly shaped neuronal cell bodies that may or may not be perfectly perpendicular to the border planes of the scan. This implies that although the majority of the signal data are from the cell observed, a certain amount of "fluorescence bleed-through" from both underneath and above could be present from neighboring cell populations, thus, giving us bit of a flawed picture of protein expression. Considering this, a great deal of attention was paid to fix the border planes of the z-stacks as close as possible to the investigated motor neurons to drastically reduce the noise. In the case of mRNA analyses, whole spinal cords were used instead of cervical regions alone. This was owing to technical difficulties involved with precise extraction of such a small specimen and very low resulting mRNA yield. The whole spinal cords contained various cell subpopulations like sensory neurons, microglia, astrocytes, and other cell types. This could, in fact, lead to lack of result supporting protein expression studies by potentially obscuring significant findings in motor neurons.

6. CONCLUSIONS AND OUTLOOK

To summarize the findings of this study, IFN-γR1 is upregulated on motor neurons from both presymptomatic and symptomatic hSOD1G93A mice. This strongly offers the possibility of increased sensitivity of the motor neurons to IFN-γ signaling, both canonical and non-canonical. Higher levels of AMPAR subunit GluR1 in motor neurons of symptomatic hSOD1G93A mice imply that the neuron-specific non-canonical IFN-γ pathway could be upregulated in disease stage in the event that the downstream targets – JAK1, STAT1, PKA – are, also, functionally upregulated. Interestingly, the expression results failed to be recapitulated in embryonic motor neurons of hSOD1G93A mice, thus, suggesting that presence of ALS mutation alone is not enough to influence the expression. Presence of dendritic beads in primary motor neurons implies neuronal damage inducing function of IFN-γ. Lack of enhanced AMPAR-mediated excitotoxicity and significant calcium signals upon IFN-γ treatment are most likely due to absence of enough strength in neurotoxicity by IFN-γ.

This study opens doors to several areas that can be explored in the future. In this piece of work, only expression studies of targets of interest were carried out in adult mice. The pathway and its functional aspects can be investigated in detail by performing experiments in adult hSOD1G93A mice. Moreover, this study can be extended to ALS patients by employing tissues collected from post-mortem cases. These studies would not only yield further insights on the interplay between neurodegeneration and neuroinflammation in ALS, but pave way to finding more therapeutic strategies as well.

7. REFERENCES

AAS, V., LARSEN, K., & IVERSEN, J.-G. (1998) IFN-γ Induces Calcium Transients and Increases the Capacitative Calcium Entry in Human Neutrophils. *J. Interf. Cytokine Res.*, **18**, 197–205.

Aebischer, J., Cassina, P., Otsmane, B., Moumen, A., Seilhean, D., Meininger, V., Barbeito, L., Pettmann, B., & Raoul, C. (2010) IFNγ triggers a LIGHT-dependent selective death of motoneurons contributing to the non-cell-autonomous effects of mutant SOD1. *Cell Death Differ.*, **18**, 754–768.

Ahmed, C.M.I. & Johnson, H.M. (2006) IFN-gamma and its receptor subunit IFNGR1 are recruited to the IFN-gamma-activated sequence element at the promoter site of IFN-gamma-activated genes: evidence of transactivational activity in IFNGR1. *J. Immunol.*, **177**, 315–321.

Bach, E.A., Aguet, M., & Schreiber, R.D. (1997) THE IFNγ RECEPTOR: A Paradigm for Cytokine Receptor Signaling. *Annu. Rev. Immunol*, **15**, 563–591.

Barish, M.E., Mansdorf, N.B., & Raissdana~, S.S. (1991) y-Interferon Promotes Differentiation of Cultured Cortical and Hippocampal Neurons. *Dev. Biol.*, **144**.

Barrett, E.F., Barrett, J.N., & David, G. (2014) Dysfunctional mitochondrial Ca2+ handling in mutant SOD1 mouse models of fALS: integration of findings from motor neuron somata and motor terminals. *Front. Cell. Neurosci.*,.

Beers, D.R., Zhao, W., Liao, B., Kano, O., Wang, J., Huang, A., Appel, S.H., & Henkel, J.S. (2011) Neuroinflammation modulates distinct regional and temporal clinical responses in ALS mice. *Brain Behav Immun*, **2512**.

Brini, M., Calì, T., Ottolini, D., & Carafoli, E. (2014) Neuronal calcium signaling: Function and dysfunction. *Cell. Mol. Life Sci.*,.

Burrell, J.R., Halliday, G.M., Kril, J.J., Ittner, L.M., Götz, J., Kiernan, M.C., Hodges, J.R., ,& al., et (2016) The frontotemporal dementia-motor neuron disease continuum. *Lancet*, **388**, 919–931.

Chen, X., Barozzi, I., Termanini, A., Prosperini, E., Recchiuti, A., Dalli, J., Mietton, F., Matteoli, G., Hiebert, S., & Natoli, G. (2012) Requirement for the histone deacetylase Hdac3 for the inflammatory gene expression program in macrophages. *Proc. Natl. Acad. Sci. U. S. A.*, **109**, E2865-74.

Choi, D.W. (1988) Glutamate Neurotoxicity and Diseases of the Nervous System. *Neuron*, **1**, 623–634.

Cook, J.R., Emanuel, S.L., Donnelly, R.J., Soh, J., Mariano, T.M., Schwartz, B., Rhee, S., & Pestka, S. (1994) Sublocalization of the human interferon-gamma receptor accessory factor gene and characterization of accessory factor activity by yeast artificial chromosomal fragmentation. *J. Biol. Chem.*, **269**, 7013–7018.

Cozzolino, M., Pesaresi, M.G., Gerbino, V., Grosskreutz, J., & Carrì, M.T. (2012) Amyotrophic Lateral Sclerosis: New Insights into Underlying Molecular Mechanisms and Opportunities for Therapeutic Intervention. *Antioxid. Redox Signal.*, **17**, 1277–1330.

Crompton, M. (1999) The mitochondrial permeability transition pore and its role in cell death. *Biochem. J.*,.

Dagda, R.K. & Das Banerjee, T. (2015) Role of protein kinase A in regulating mitochondrial function and neuronal development: implications to neurodegenerative diseases. *Rev. Neurosci.*, **26**, 359–370.

Darnell, J.E., Kerr, I.M., & Stark, G.R. (1994) Jak-STAT Pathways and Transcriptional Activation in Response to IFNs and Other Jak-STAT Pathways and Transcriptional Activation in Response to IFNs and Other Extracellular Signaling Proteins. *Source Sci. New Ser.*, **264**, 1415–1421.

Daroff, R.B., Fenichel, G.M., Jankovic, J.J., & Mazziotta, J.C. (2012) *Bradley's Neurology*, Bradley Neurology.

DECKER, T., KOVARIK, P., & MEINKE, A. (1997) GAS Elements: A Few Nucleotides with a Major Impact on Cytokine-Induced Gene Expression. *J. Interf. Cytokine Res.*, **17**, 121–134.

Delisle, M.B. & Carpenter, S. (1984) Neurofibrillary axonal swellings and amyotrophic lateral sclerosis. *J. Neurol. Sci.*, **63**, 241–250.

Dickson, T.C., King, C.E., McCormack, G.H., & Vickers, J.C. (1999) Neurochemical diversity of dystrophic neurites in the early and late stages of Alzheimer's disease. *Exp. Neurol.*, **156**, 100–110.

Dong, X.-X., Wang, Y., & Qin, Z.-H. (2009) Molecular mechanisms of excitotoxicity and their relevance to pathogenesis of neurodegenerative diseases. *Acta Pharmacol Sin Acta Pharmacol. Sin.*, **30**, 379–387.

Eisen, A. & Weber, M. (2001) The motor cortex and amyotrophic lateral sclerosis. *Muscle Nerve*,.

Farrar, M.A. & Schreiber, R.D. (1993) THE MOLECULAR CELL BIOLOGY OF INTERFERON-y AND ITS RECEPTOR. *Annu. ReI'. Immunol*, **11**, 571–611.

Fenn, A.M., Norden, D.M., & Godbout, J.P. (2015) Neuroinflammation in Aging. In *Neuroinflammation*. John Wiley & Sons, Inc, Hoboken, NJ, USA, pp. 87–105.

Ferrari, R., Kapogiannis, D., Huey, E.D., & Momeni, P. (2011) FTD and ALS: a tale of two diseases. *Curr. Alzheimer Res.*, **8**, 273–294.

Fourgeaud, L., Davenport, C.M., Tyler, C.M., Cheng, T.T., Spencer, M.B., & Boulanger, L.M. (2010) MHC class I modulates NMDA receptor function and AMPA receptor trafficking. *Proc. Natl. Acad. Sci. U. S. A.*, **107**, 22278–22283.

Franciosi, S., Choi, H.B., Kim, S.U., & McLarnon, J.G. (2002) Interferon-γ acutely induces calcium influx in human microglia. *J. Neurosci. Res.*, **69**, 607–613.

Gavet, O. & Pines, J. (2010) Activation of cyclin B1-Cdk1 synchronizes events in the nucleus and the cytoplasm at mitosis. *J. Cell Biol.*, **189**, 247–259.

Goel, S., Wharton, S.B., Brett, L.P., & Whittle, I.R. (2003) Morphological changes and stress responses in neurons in cerebral cortex infiltrated by diffuse astrocytoma. *Neuropathology*, **23**, 262–270.

Gordon, P.H., Cheng, B., Salachas, F., Pradat, P.F., Bruneteau, G., Corcia, P., Lacomblez, L., & Meininger, V. (2010) Progression in ALS is not linear but is curvilinear. *J. Neurol.*,.

Greger, I.H., Ziff, E.B., & Penn, A.C. (2007) Molecular determinants of AMPA receptor subunit assembly. *Trends Neurosci.*,.

Grosskreutz, J., Haastert, K., Dewil, M., Van Damme, P., Callewaert, G., Robberecht, W., Dengler, R., & Van Den Bosch, L. (2007) Role of mitochondria in kainate-induced fast Ca2+ transients in cultured spinal motor neurons. *Cell Calcium*, **42**, 59–69.

Grosskreutz, J., Van Den Bosch, L., & Keller, B.U. (2010) Calcium dysregulation in amyotrophic lateral sclerosis. *Cell Calcium*, **47**, 165–174.

Gunter, T.E. & Sheu, S.-S. (2009) Characteristics and possible functions of mitochondrial Ca(2+) transport mechanisms. *Biochim. Biophys. Acta*,.

Gurney, M., Pu, H., Chiu, A., Dal Canto, M., Polchow, C., Alexander, D., Caliendo, J., Hentati, A., Kwon, Y., Deng, H., & et, al. (1994) Motor neuron degeneration in mice that express a human Cu,Zn superoxide dismutase mutation. *Science (80-.).*, **264**.

Hansen ', A.B., Bouchelouche2, P.N., Lillevang3, S.T., & Andersen ', C.B. (1994) Interferon-gamma increases cellular calcium ion concentration and inositol 1,4,5-trisphosphate formation in human renal carcinoma cells: relation to ICAM-1 antigen expression **69**,

291–298.

Hasbani, M.J., Hyrc, K.L., Faddis, B.T., Romano, C., & Goldberg, M.P. (1998) Distinct Roles for Sodium, Chloride, and Calcium in Excitotoxic Dendritic Injury and Recovery. *Exp. Neurol.*, **154**, 241–258.

Hibino, Y., Mariano, T.M., Kumar, C.S., Kozak, C.A., & Pestka, S. (1991) Expression and reconstitution of a biologically active mouse interferon γ receptor in hamster cells: Chromosomal location of an accessory factor. *J. Biol. Chem.*, **266**, 6948–6951.

Hori, N. & Carpenter, D.O. (1994) Functional and Morphological Changes Induced by Transient in Vivo Ischemia. *Exp. Neurol.*, **129**, 279–289.

Hu, J.H., Chernoff, K., Pelech, S., & Krieger, C. (2003) Protein kinase and protein phosphatase expression in the central nervous system of G93A mSOD over-expressing mice. *J. Neurochem.*, **85**, 422–431.

Inglis, F.M., Crockett, R., Korada, S., Abraham, W.C., Hollmann, M., & Kalb, R.G. (2002) The AMPA receptor subunit GluR1 regulates dendritic architecture of motor neurons. *J. Neurosci.*,.

Jaenisch, N., Liebmann, L., Guenther, M., Hübner, C.A., Frahm, C., & Witte, O.W. (2016) Reduced tonic inhibition after stroke promotes motor performance and epileptic seizures. *Sci. Rep.*, **6**, 26173.

Jakowec, M.W., Fox, A.J., Martin, L.J., & Kalb, R.G. (1995) Quantitative and qualitative changes in AMPA receptor expression during spinal cord development. *Neuroscience*, **67**, 893–907.

Jakowec, M.W., Yen, L., & Kalb, R.G. (1995) In situ hybridization analysis of AMPA receptor subunit gene expression in the developing rat spinal cord. *Neuroscience*, **67**, 909–920.

Kim, I.-J., Beck, H.N., Lein, P.J., & Higgins, D. (2002) Interferon gamma induces retrograde dendritic retraction and inhibits synapse formation. *J. Neurosci.*, **22**, 4530–4539.

King, A.E., Woodhouse, A., Kirkcaldie, M.T.K., & Vickers, J.C. (2016) Excitotoxicity in ALS: Overstimulation, or overreaction?

Kirby, J., Al Sultan, A., Waller, R., & Heath, P. (2016) The genetics of amyotrophic lateral sclerosis: current insights. *Degener. Neurol. Neuromuscul. Dis.*, **6**, 49.

Krämer, O.H., Knauer, S.K., Greiner, G., Jandt, E., Reichardt, S., Gührs, K.-H., Stauber, R.H., Böhmer, F.D., & Heinzel, T. (2009) A phosphorylation-acetylation switch regulates STAT1 signaling. *Genes Dev.*, **23**, 223–235.

Kulkarni, A., Ganesan, P., & O'Donnell, L.A. (2016) Interferon Gamma: Influence on Neural Stem Cell Function in Neurodegenerative and Neuroinflammatory Disease. *Clin. Med. Insights. Pathol.*, **9**, 9–19.

Kung, A.W., Lau, K.S., & Wong, N.S. (1995) Interferon-gamma increases intracellular calcium and inositol phosphates in primary human thyroid cell culture. *Endocrinology*, **136**, 5028–5033.

Liu, J., Gao, L., & Zang, D. (2015) Elevated Levels of IFN-γ in CSF and Serum of Patients with Amyotrophic Lateral Sclerosis. *PLoS One*, **10**, e0136937.

Liu, J. & Wang, F. (2017) Role of Neuroinflammation in Amyotrophic Lateral Sclerosis: Cellular Mechanisms and Therapeutic Implications. *doi.org*, **8**, 1005.

Londino, J.D., Gullick, D.L., Lear, T.B., Suber, T.L., Weathington, N.M., Masa, L.S., Chen, B.B., & Mallampalli, R.K. (2017) Post-translational modification of the interferon gamma receptor alters its stability and signaling. *Biochem. J.*, BCJ20170548.

Martinez, F.O. & Gordon, S. (2014) The M1 and M2 paradigm of macrophage activation: time for reassessment. *F1000Prime Rep.*, **6**, 13.

Martino, G., Brambilla, E., Filippi, M., Martinelli, V., Colombo, B., Rodegher, M., Comi, G., & Grimaldi, L.M. (1996) Interferon-gamma activated calcium influx in peripheral blood lymphocytes from patients with primary and secondary progressive multiple sclerosis. *J. Neurol. Neurosurg. Psychiatry*, **61**, 515–517.

Mattila, P.M., Rinne, J.O., Helenius, H., Dickson, D.W., & Röyttä, M. (2000) Alpha-synuclein-immunoreactive cortical Lewy bodies are associated with cognitive impairment in Parkinson's disease. *Acta Neuropathol.*, **100**, 285–290.

Mayer, M.L. (2005) Glutamate receptor ion channels. *Curr. Opin. Neurobiol.*,.

Michaelson, N., Facciponte, D., Bradley, W., & Stommel, E. (2017) Cytokine expression levels in ALS: A potential link between inflammation and BMAA-triggered protein misfolding.

Mizuno, T., Zhang, G., Takeuchi, H., Kawanokuchi, J., Wang, J., Sonobe, Y., Jin, S., Takada, N., Komatsu, Y., & Suzumura, A. (2008) Interferon-γ directly induces neurotoxicity through a neuron specific, calcium-permeable complex of IFN-γ receptor and AMPA GluR1 receptor. *FASEB J.*, **22**, 1797–1806.

Muller, M., Laxton, C., Briscoe, J., Schindler1, C., Lmprota2, T., Darnell, J.E., Stark3, G.R., & Kerr, I.M. (1993) Complementation of a mutant cell line: central role of the 91 kDa polypeptide of ISGF3 in the interferon-oe and --y signal transduction pathways. *EMBO*

J., **1**, 4221–4228.

Nardo, G., Trolese, M.C., & Bendotti, C. (2016) Major Histocompatibility Complex I Expression by Motor Neurons and Its Implication in Amyotrophic Lateral Sclerosis. *Front Neurol*,.

O'Donnell, L.A., Henkins, K.M., Kulkarni, A., Matullo, C.M., Balachandran, S., Pattisapu, A.K., & Rall, G.F. (2015) Interferon gamma induces protective non-canonical signaling pathways in primary neurons. *J. Neurochem.*, **135**, 309–322.

Patai, R., Nógrádi, B., Engelhardt, J.I., & Siklós, L. (2016) Calcium in the pathomechanism of amyotrophic lateral sclerosis - Taking center stage? *Biochem. Biophys. Res. Commun.*,.

Pernis, A., Gupta, S., Gollob, K.J., Garfein, E., Coffman, R.L., Schindler, C., & Rothman, P. (1995) Lack of interferon γ receptor β chain and the prevention of interferon γ signaling in TH1 Cells. *Science (80-.).*, **269**, 245–247.

Pestka, S., Serguei, S., Kotenko, V., Muthukumaran, G., Izotova, L.S., Cook, J.R., & Garottat, G. (1997) The Interferon Gamma (IFN-y) Receptor: a Paradigm for the Multichain Cytokine Receptor. *~h Fwtor Rerkw*, **8**.

Pfaffl, M.W. (2001) A new mathematical model for relative quantification in real-time RT-PCR. *Nucleic Acids Res.*, **29**, e45.

Philips, T., Robberecht, W., Ringholz, G., Appel, S., Bradshaw, M., Cooke, N., Mosnik, D., Schulz, P., Damme, P. Van, & al., et (2011) Neuroinflammation in amyotrophic lateral sclerosis: role of glial activation in motor neuron disease. *Lancet. Neurol.*, **10**, 253–263.

Poesen, K., De Schaepdryver, M., Stubendorff, B., Gille, B., Muckova, P., Wendler, S., Prell, T., Ringer, T.M., Rhode, H., Stevens, O., Claeys, K.G., Couwelier, G., D'hondt, A., Lamaire, N., Tilkin, P., Van Reijen, D., Gourmaud, S., Fedtke, N., Heiling, B., Rumpel, M., Rödiger, & al., et. (2017) Neurofilament markers for ALS correlate with extent of upper and lower motor neuron disease. *Neurology*,.

Prithviraj, R., Kelly, K.M., Espinoza-Lewis, R., Hexom, T., Clark, A.B., & Inglis, F.M. (2007) Differential Regulation of Dendrite Complexity by AMPA Receptor Subunits GluR1 and GluR2 in Motor Neurons. *Inc. Dev. Neurobiol*, **68**, 247–264.

Reaume, A.G., Elliott, J.L., Hoffman, E.K., Kowall, N.W., Ferrante, R.J., Siwek, D.F., Wilcox, H.M., Flood, D.G., Beal, M.F., Brown, R.H., Scott, R.W., & Snider, W.D. (1996) Motor neurons in Cu/Zn superoxide dismutase-deficient mice develop normally but exhibit enhanced cell death after axonal injury. *Nat. Genet.*,.

Saito, Y., Kawashima, A., Ruberu, N.N., Fujiwara, H., Koyama, S., Sawabe, M., Arai, T.,

Nagura, H., & al, et. (2003) Accumulation of phosphorylated alpha-synuclein in aging human brain. *J. Neuropathol. Exp. Neurol.*, **62**, 644–654.

Schoenborn, J.R. & Wilson, C.B. (2007) Regulation of Interferon-γ During Innate and Adaptive Immune Responses. *Adv. Immunol.*, **96**, 41–101.

Shuai, K., Schindler, C., Prezioso, V., & Darnell, J. (1992) Activation of transcription by IFN-gamma: tyrosine phosphorylation of a 91-kD DNA binding protein. *Science (80-.).*, **258**, 1808–1812.

Soh, J., Donnelly, R.J., Kotenko, S., Mariano, T.M., Cook, J.R., Wang, N., Emanuel, S., Schwartz, B., Miki, T., & Pestka, S. (1994) Identification and sequence of an accessory factor required for activation of the human interferon γ receptor. *Cell*, **76**, 793–802.

Song, J.H., Wang, C.X., Song, D.K., Wang, P., Shuaib, A., & Hao, C. (2005) Interferon Induces Neurite Outgrowth by Up-regulation of p35 Neuron-specific Cyclin-dependent Kinase 5 Activator via Activation of ERK1/2 Pathway*.

Song, S., Miranda, C.J., Braun, L., Meyer, K., Frakes, A.E., Ferraiuolo, L., Likhite, S., Bevan, A.K., Foust, K.D., McConnell, M.J., Walker, C.M., & Kaspar, B.K. (2016) Major histocompatibility complex class I molecules protect motor neurons from astrocyte-induced toxicity in amyotrophic lateral sclerosis. *Nat. Med.*, **22**, 397–403.

Stellwagen, D., Beattie, E.C., Seo, J.Y., & Malenka, R.C. (2005) Differential regulation of AMPA receptor and GABA receptor trafficking by tumor necrosis factor-alpha. *J. Neurosci.*, **25**, 3219–3228.

Stutzmann, G.E. & Mattson, M.P. (2011) Endoplasmic reticulum Ca(2+) handling in excitable cells in health and disease. *Pharmacol. Rev.*, **63**, 700–727.

Swann, J.W., Al-Noori, S., Jiang, M., & Lee, C.L. (2000) Spine loss and other dendritic abnormalities in epilepsy. *Hippocampus*, **10**, 617–625.

Swinnen, B. & Robberecht, W. (2014) The phenotypic variability of amyotrophic lateral sclerosis. *Nat. Publ. Gr.*, **10**.

Tadic, V., Prell, T., Lautenschlaeger, J., Grosskreutz, J., Kristian, T., & Berger, H. (2014) The ER mitochondria calcium cycle and ER stress response as therapeutic targets in amyotrophic lateral sclerosis.

Takahashi, T., Yagishita, S., Amano, N., Yamaoka, K., & Kamei, T. (1997) Amyotrophic lateral sclerosis with numerous axonal spheroids in the corticospinal tract and massive degeneration of the cortex. *Acta Neuropathol.*, **94**, 294–299.

Takeuchi, H., Mizuno, T., Zhang, G., Wang, J., Kawanokuchi, J., Kuno, R., & Suzumura, A.

(2005) Neuritic beading induced by activated microglia is an early feature of neuronal dysfunction toward neuronal death by inhibition of mitochondrial respiration and axonal transport. *J. Biol. Chem.*, **280**, 10444–10454.

Talbott, E.O., Malek, A.M., & Lacomis, D. (2016) The epidemiology of amyotrophic lateral sclerosis. *Handb. Clin. Neurol.*, **138**, 225–238.

Taylor, J.P., Brown, R.H., & Cleveland, D.W. (2016) Decoding ALS: From genes to mechanism. *Nature*,.

Van Damme, P., Callewaert, G., Eggermont, J., Robberecht, W., & Van Den Bosch, L. (2003) Chloride influx aggravates Ca2+-dependent AMPA receptor-mediated motoneuron death. *J. Neurosci.*, **23**, 4942–4950.

Van Den Bosch, L., Van Damme, P., Bogaert, E., & Robberecht, W. (2006) The role of excitotoxicity in the pathogenesis of amyotrophic lateral sclerosis. *Biochim. Biophys. Acta - Mol. Basis Dis.*,.

Van Den Bosch, L., Vandenberghe, W., Klaassen, H., Van Houtte, E., & Robberecht, W. (2000) Ca2+-permeable AMPA receptors and selective vulnerability of motor neurons. *J. Neurol. Sci.*, **180**, 29–34.

Verkhratsky, A. (2005) Physiology and Pathophysiology of the Calcium Store in the Endoplasmic Reticulum of Neurons. *Physiol. Rev.*,.

Walter, M.R., Windsor, W.T., Nagabhushan, T.L., Lundell, D.J., Lunn, C. a, Zauodny, P.J., & Narula, S.K. (1995) Crystal structure of a complex between interferon-gamma and its soluble high-affinity receptor. *Nature*, **376**, 230–235.

Weishaupt, J.H., Hyman, T., & Dikic, I. (2016) Common Molecular Pathways in Amyotrophic Lateral Sclerosis and Frontotemporal Dementia. *Trends Mol. Med.*, **22**, 769–783.

Yoshihara, T., Ishigaki, S., & Yamamoto, M. (2001) Differential expression of inflammationand apoptosis-related genes in spinal cords of a mutant SOD1 transgenic mouse model of familial amyotrophic lateral sclerosis. *J. Neurochem.*, **VH,** 158±167.

Zhao, P., Ignacio, S., Beattie, E.C., & Abood, M.E. (2008) Altered presymptomatic AMPA and cannabinoid receptor trafficking in motor neurons of ALS model mice: implications for excitotoxicity. *Eur. J. Neurosci.*, **27**, 572–579.

Zwiegers, P. & Shaw, C.A. (2015) Disparity of outcomes: the limits of modeling amyotrophic lateral sclerosis in murine models and translating results clinically. *J. Controv. Biomed. Res.*, **1**, 4–22.

8. APPENDIX

8.1 List of Figures

8.2 List of Tables

8.3 Acknowledgements

At the outset, I'd like to express my deepest gratitude to my supervisor PD. Dr. med. Julian Grosskreutz for giving me the opportunity to conduct my PhD in his group. His guidance and continuous support, patience, motivation, and immense knowledge helped me greatly during my PhD time. Thank you. I am, also, very grateful to my co-supervisor Prof. Dr. Otto W. Witte for bringing me into his department and providing me with excellent working conditions alongwith constructive suggestions and support during the progress meetings.

My sincere thanks to my lab colleagues for their technical support throughout the years -- especially to Svetlana Tausch for her technical expertise on tissue preparation alongwith Madlen Gunther and Dr. Christiane Frahm for their help with qPCR. I would, also, like to thank my lab mates for their support with my experimental work, especially to Thanh Tu Le, Adam Adam, and Vedrana Tadic. Additionally, I'd like to express my heartfelt gratitude to Dr. Beatrice Stubbendorf, Dr. Silke Keiner and Jingju Liu for the stimulating discussions and their moral support during lab meetings.

Friendship that I shared with Jefri, Preetha, Jelena, Danica, Shivali, and Nayana during long working hours was comforting and empowering. I am also thankful to Nasim Kroegel, our project manager for her support with administrative matters during my time in the Department.

I am truly grateful to all the members of the Department of Neurology for their expert inputs in the form of scientific questions during progress meetings and the pleasant working atmosphere. To Prof. Dr. Regine Heller and IZKF, I cannot thank enough for the immense effort in organising the Summer School that brought me to Jena. I had, also, like to give a shout-out to all my summer school friends who supported me and made the time out of the lab enjoyable. I am thankful to all the previous colleagues, teachers, and professors for the enriching professional journey so far. And last of all, I am exceedingly thankful to my family, especially my loving parents and sister for always believing in me and encouraging me throughout my life.

8.4 Curriculum Vitae

Saikata Sengupta
AG NEDIG
Department of Neurology, Jena University Hospital
Am Klinikum 1, 07747 Jena, Germany
Phone: +49 17682215424
E-Mail: Saikata.Sengupta@med.uni-jena.de

EDUCATION

PhD Candidate – Department of Neurology, Faculty of Medicine **2014-present**
Jena University Hospital, Germany Degree expected in February 2019

M.Sc. in Biomedical Genetics **2009-2011**
Vellore Institute of Technology, India GPA: **8.66/10.00**

- *Thesis: Isolation and purification of recombinant mammalian transcription factor IRF-2*

B.Sc in Microbiology **2006-2009**
University of Madras, India Aggregate: **75.5%**

HONORS & AWARDS

FZL Young Scientists Day award Best poster presentation	Jena University Hospital, Germany	**2018**
PROCHANCE grant Awarded to selected young female scientists for scientific exchange	Friedrich Schiller University, Germany	**2016 & 2018**
FAZIT-Stiftung Travel Grant Awarded to selective candidates to participate in conferences	FAZIT Foundation, Germany	**2017**
IZKF PhD fellowship Awarded to best summer school student	IZKF, Jena University Hospital, Germany	**2014**
DAAD fellowship Awarded to top 25 students globally	Summer School of Medicine, Jena University Hospital, Germany	**2014**
College Endowment Award Awarded for outstanding academic achievement	Madras University, India	**2009**

Proficiency Awards Madras University, India **2006-2009**
For topping every semester of undergraduation in all courses

WORK EXPERIENCE

Science communicator for Neuroscience and Artificial Intelligence **April 2018- Present**

Massive Science Inc.

Blogger for Neuroscience and Artificial Intelligence **August 2017- March 2018**

Club SciWri

Research Assistant **August 2013 - August 2014**

Indian Institute of Science, India

- Focused on the role of CG9650 gene in corticospinal neuron development in *Drosophila melanogaster*

Research Assistant **August 2012 - June 2013**

University of Cincinnati College of Medicine, USA

- Focused on the PRDC protein that is a BMP (Bone Morphogenetic Protein) antagonist and plays an important role in the TGF-beta signaling.

Faculty member for THOTS **June 2011- February 2012**

Mindedutainement Pvt. Ltd., India

- Responsibilities included initiating and developing cognitive, social and emotional skills among school children via different strategies, assessing each student's progress and devising ways for improvement.

Research Trainee **June 2010 - July 2010**

Shantha Biotech Ltd. (Parent Co.: Sanofi Aventis Global), India

- Worked in the Vaccine Formulation division of the organization. Responsibilities included designing formulations for vaccines like HPV, DPT, TT; testing the shelf-life of the formulated vaccines and optimizing the same.

PRESENTATIONS & PUBLISHED ABSTRACTS

ENCALS 2018, Oxford, UK. Neuron-specific non-canonical IFN-gamma pathway in ALS. **Saikata Sengupta**, Thanh Tu Le, Vedrana Tadic, Silke Keiner, Beatrice Stubendorff, Tino Prell, Otto W Witte, Julian Grosskreutz.

28th International Symposium on ALS/MND, Boston, USA. Impact of interferon-gamma on neurotoxicity and the ER mitochondria coupling cycle in G93A SOD1 mouse embryonic motor neurons **S Sengupta**, V Tadic, A Malci, TT Le, B Stubendorff, T Prell, S Keiner, J Grosskreutz.

27th International Symposium on ALS/MND, Dublin, Ireland. Impact of interferon-gamma on neurotoxicity and the ER mitochondria coupling cycle in ALS. **S Sengupta**, S Keiner, V Tadic, A Malci, TT Le, B Stubendorff, OW Witte, T Prell, J Grosskreutz.

27th International Symposium on ALS/MND, Dublin, Ireland. Role of the mitochondrial Na/Ca/Li-Exchanger (NCLX) in the pathophysiology of ALS. TT Le, S Keiner, V Tadic, **S Sengupta**, A Malci, B Stubendorff, OW Witte, T Prell, J Grosskreutz.

ENCALS 2016, Milan, Italy. Impact of IFN-© on neurotoxicity and ER-mitochondria coupling cycle in ALS. **Sengupta S**, Tadic V, Malci A, Liu J, Le TT, Stubendorff B, Witte OW, Prell T, Grosskreutz J.

ENCALS 2016, Milan, Italy. Role of the mitochondrial Na/Ca/Li-exchanger (NCLX) in the pathophysiology of ALS. Le TT, Keiner S, Tadic V, Malci A, Liu J, **Sengupta S**, Stubendorff B, Witte OW, Prell T, Grosskreutz J.

PUBLICATIONS

1. Non-canonical neuron-specific Interferon-gamma pathway in ALS. **First author publication. Accepted with minor revision at European Journal of Neuroscience.**
2. Sigma 1 receptor activation modifies intracellular calcium exchange in the $G93A^{hSOD1}$ ALS model. (Tadic, V et al., 2017). *Neuroscience. Volume 359, 17 September 2017, Pages 105-118.*

LEADERSHIP

- Main coordinator for organizing workshops, training sessions, and creating appropriate documentation for IncuCyte live-cell analysis imaging system among 3 departments at the Jena University Hospital, Germany.
- Supervised MD (Doctor of Medicine) students in our group for their research projects during my PhD.
- Organized meetups in Europe for STEMPEERS, world's biggest network of STEM professionals.
- Chief Coordinator and host for fests and other stage events like national seminars during graduation
- Editor of college magazine during graduate education in India

COMPETENCIES

Spinal cord & brain slice, primary neuron-glial cell culture, NSC-34 and iPSC cells, calcium imaging, confocal microscopy, western blot, immunohistochemistry, IncuCyte live-cell imaging, PCR, cloning, chromatography, protein isolation and purification, Image J, Fiji, Python programming, GraphPad.

8.5 Ehrenwörtliche Erklärung

Hiermit erkläre ich, dass mir die Promotionsordnung der Medizinischen Fakultät der Friedrich-Schiller-Universität bekannt ist,

ich die Dissertation selbst angefertigt habe und alle von mir benutzten Hilfsmittel, persönlichen Mitteilungen und Quellen in meiner Arbeit angegeben sind,

dass die Personen, die mich bei der Auswahl und Auswertung des Materials sowie bei der Herstellung des Manuskripts unterstützt haben, vollständig genannt sind,

die Hilfe eines Promotionsberaters nicht in Anspruch genommen wurde und dass Dritte weder unmittelbar noch mittelbar geldwerte Leistungen von mir für Arbeiten erhalten haben, die im Zusammenhang mit dem Inhalt der vorgelegten Dissertation stehen,

dass ich die Dissertation noch nicht als Prüfungsarbeit für eine staatliche oder andere wissenschaftliche Prüfung eingereicht habe und dass ich die gleiche, eine in wesentlichen Teilen ähnliche oder eine andere Abhandlung nicht bei einer anderen Hochschule als Dissertation eingereicht habe

Diese Dissertation wird mit einer kleinen Überarbeitung zur Publikation angenommen. (Siehe Appendix, 8.4. Publications).

Jena, 27.06.2017 Unterschrift des Verfassers